NASA CONTRACTOR REPORT

NASA CR-2753

STUDIES OF EARTH SIMULATION EXPERIMENTS

John E. Hart

Prepared by
MASSACHUSETTS INSTITUTE OF TECHNOLOGY
Cambridge, Mass. 02139
for George C. Marshall Space Flight Center

NATIONAL AERONAUTICS AND SPACE ADMINISTRATION • WASHINGTON, D. C. • OCTOBER 1976

1. REPORT NO.	2. GOVERNMENT ACCESSION NO.	3. RECIPIENT
NASA CR-2753		

4. TITLE AND SUBTITLE	5. REPORT DATE
Studies of Earth Simulation Experiments	October 1976
	6. PERFORMING ORGANIZATION CODE

7. AUTHOR(S)	8. PERFORMING ORGANIZATION REPORT #
John E. Hart	M-181

9. PERFORMING ORGANIZATION NAME AND ADDRESS	10. WORK UNIT NO.
Department of Meteorology Massachusetts Institute of Technology Cambridge, Massachusetts 02139	11. CONTRACT OR GRANT NO. NAS8-31149
	13. TYPE OF REPORT & PERIOD COVERED Contractor Report
12. SPONSORING AGENCY NAME AND ADDRESS National Aeronautics and Space Administration Washington, D. C. 20546	14. SPONSORING AGENCY CODE

15. SUPPLEMENTARY NOTES

This report was prepared under the technical monitorship of the Aerospace Environment Division, Space Sciences Laboratory, Marshall Space Flight Center.

16. ABSTRACT

The "low gravity" environment of Earth orbit offers the potential for performing experiments involving baroclinic geophysical fluid dynamics (GFD) on spherical surfaces. These experiments in turn have the potential for providing deeper understanding of large-scale planetary and solar circulations. However, to perform these experiments, one requires an experimental technique whereby a radially directed body force can be generated to simulate a radial gravitational force field. One viable technique is the use of dielectric fluids with temperature dependent dielectric permittivity in a radially directed electric field. Application of the Boussinesq approximation to the equations of motion for this system and restrictions on the size of certain electrodynamic terms in the energy equations yields a set of equations which are analogous to the equations of motions of geophysical systems like the Earth's atmosphere on term-by-term basis. This report describes the theoretical design of GFD experiments for performance in Earth orbit along with results of preliminary tests of a prototype.

17. KEY WORDS	18. DISTRIBUTION STATEMENT
Geophysical fluid dynamics Dynamic meteorology Climate	Category 47

19. SECURITY CLASSIF. (of this report)	20. SECURITY CLASSIF. (of this page)	21. NO. OF PAGES	22. PRICE
Unclassified	Unclassified	73	$ 4.25

For sale by the National Technical Information Service, Springfield, Virginia 22161

FOREWORD

The research reported herein was supported by NASA Contract NAS8-31149. Dr. George H. Fichtl and Dr. William C. Cliff of the Aerospace Environment Division, Space Sciences Laboratory, Marshall Space Flight Center, were the scientific monitors, and support was provided by the NASA Office of Applications, Earth Observation Programs and Meteorology.

The research reported in this document is concerned with the design of geophysical fluid dynamics (GFD) experiments of major scientific importance which require the unique "low-gravity" environment of Earth orbit to be successfully performed. The experiments offer the opportunity to study baroclinic fluid flows on rotating spherical surfaces with an imposed radially directed body force to simulate a gravitational force field. Comparable terrestrial baroclinic GFD experiments have been restricted to cylindrical geometry, and thus to the study of β-plane flow situations. Accordingly, Earth orbit offers the potential for a major step forward in GFD research which in turn may lead to new understanding of the planetary-scale dynamics of atmospheric flows.

TABLE OF CONTENTS

LIST OF FIGURES

LIST OF TABLES

1. Introduction

Meteorologists and astrophysicists interested in large-scale planetary and solar circulations have come to recognize the importance of rotation and stratification in determining the character of these flows. In particular, the effect of latitude-dependent Coriolis force on nonlinear convection is thought to play a crucial role in such phenomena as differential rotation on the sun, cloud band orientation on Jupiter, and the generation of magnetic fields in thermally driven dynamos. Most theoretical and all experimental work on these problems has in the past treated only local curvature effects--the mid-latitude or equatorial β-planes of meteorology being well-known examples. In fact, terrestrial laboratory experiments have only been able to study β-plane flows in situations where the stratification is extremely simple, usually two layers of fluid of slightly different density (see Hart, 1972). Even here only local curvature effects occurring near the poles can be modelled. One cannot model equatorial regions where the rotation axis is perpendicular to gravity because then the earth's gravity field becomes an oscillatory force in the coordinates rotating with the body. Other body forces proportional to density can be generated in the laboratory. One simple example is the centrifugal buoyancy force which is perpendicular to the rotation axis. Thus if a body is rotated rapidly enough, this centrifugal force can dominate regular gravitational effects and a dynamical approximation to the equatorial plane can be achieved.

This effect has been used by Busse, et. al., (1974) to study rotational effects on equatorial convection. However, this analogy extends to non-equatorial latitudes only when the body rotates so fast that rotational constraints are dominant everywhere (e.g., as the Taylor number T_a, defined below, becomes ∞). The values of T_a appropriate to the astrophysical flows we wish to study are thought to be in the range 10^2 to 10^6 (Gilman, 1974). The latter is a strong (possibly but not dominant) rotational limit, while the former is a weak rotation case. Clearly we need to study both limits in order to gain understanding of geophysically relevant flows. The key to physical experimentation on this subject is the generation of buoyancy forces which are radially rather than axially or uniformly directed. This report describes the theoretical design of such an experiment along with results of preliminary laboratory tests of a prototype.

2. Theoretical foundations

In trying to construct a physical laboratory analog to a geophysical flow it almost always proves impossible to maintain geometrical and dynamical similarity in all respects with known materials and techniques. The case of deep, convecting, rotating, planetary or solar atmospheres is no exception. We take the point of view that we will make a laboratory simulation of a system which is in many respects similar to the natural ones we are interested in, but in which already some processes are neglected. The fundamental system we take is that of Boussinesq

liquid contained in a rotating spherical annulus with thermal forcing (which may be latitude dependent) imposed at inner and outer spherical surfaces. The configuration is shown in Figure I. The body rotates at rate Ω and contains a heated annulus of κ, ν, α-type fluid. The following parameters describe the system and fluid.

Table I
Fluid parameters and geometry

r	radial coordinate
θ	longitude
ϕ	latitude
Ω	basic rotation rate
κ	thermal diffusivity
ν	kinematic viscosity
α	coefficient of volume expansion
R_i	inner radius
R_o	outer radius
P	pressure
$\underset{\sim}{u}$	velocity vector
ρ_o	background mean density
T	temperature relative to ambient

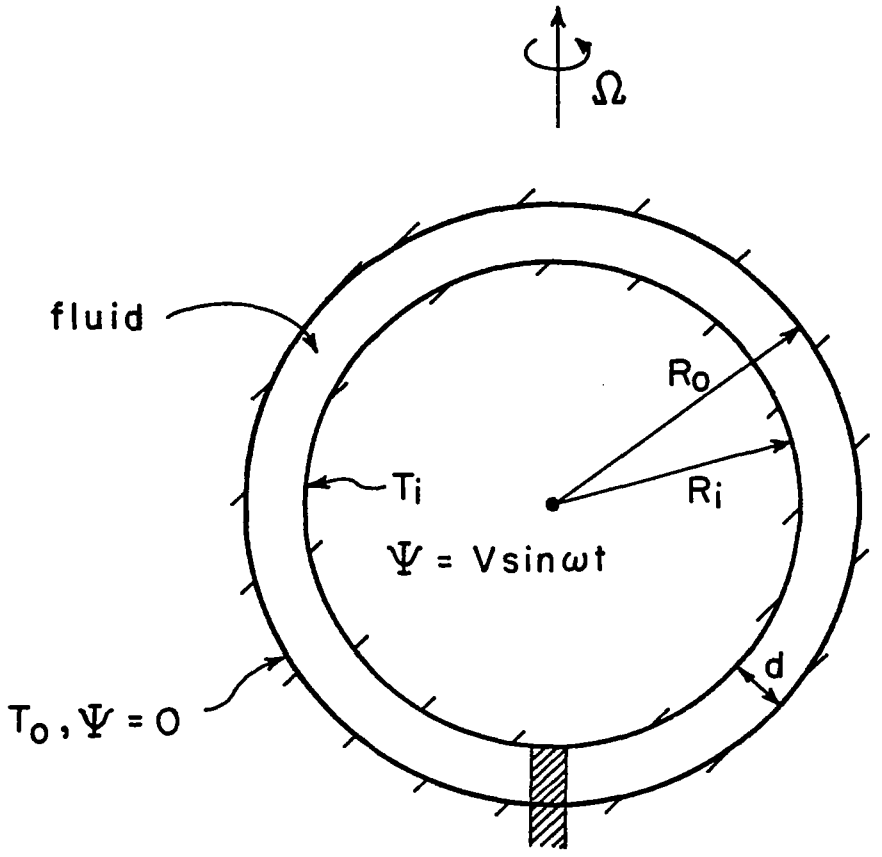

Figure 1. Geometry of the rotating spherical shell experiment. The outer shell at radius R_o is maintained at temperature T_o, voltage $\Psi = 0$. The inner shell at radius R_i is at temperature T_i voltage V sin ωt. The applied frequency is 60 hz. The temperature difference $\Delta T = T_i - T_o$ (> 0 for unstable convection). The whole apparatus is rotated about its axis. The interior is fed via a supporting neck.

The dimensional equations in this Boussinesq fluid model are:

$$\rho_o \left[\frac{d\underset{\rightarrow}{u}}{dt} + 2\underset{\rightarrow}{\Omega} \times \underset{\rightarrow}{u} \right] = -\nabla P + g(r)\alpha\rho_o T \hat{r} + \nu \nabla^2 \underset{\rightarrow}{u} \quad * \tag{2.1}$$

$$\frac{dT}{dt} = \kappa \nabla^2 T \tag{2.2}$$

$$\nabla \cdot \underset{\rightarrow}{u} = 0. \tag{2.3}$$

Note that the buoyancy force acts in the radial direction with a given gravitational acceleration g(r). We wish to construct a laboratory analog of the flow situation described by these equations.

Let us first note the well known assumptions used in deriving (2.1) - (2.3) from the full non-linear Navier-Stokes equations.

1. The Mach number is small
2. The height scale for the motion is small compared with the atmospheric scale height.

In addition to applying these incompressible equations to a deep compressible gas we also assume that small scale turbulence can be represented by uniform "eddy" viscosities and diffusivities. One might want to add small scale turbulence (occurring at scales << d), magnetic fields, radiative transfer, and compressibility, to make this mathematical model more realistic. However the possibility of constructing a laboratory

---

*For conciseness we denote frictional terms as "∇^2" recalling that in different coordinates the divergence of the viscous stress tensor includes new terms.

analog with all these added physical elements is extremely remote.

Equations (2.1) - (2.3) apply to subsonic convective motions of a shallow rotating atmosphere when α is replaced by Θ_0^{-1}, the inverse background potential temperature and T by Θ. The equations stand as written for all subsonic oceanic motions except where different diffusivities of salt and heat are important. Thus a laboratory model based on these equations will have a wide range of applicability to many different geophysical situations.

Another reason for starting with eqns. (2.1) - (2.3) is that they serve as the governing equations for most theoretical studies of planetary and solar circulations and contain much of the key physics without added complexity of the other effects. While it is admittedly risky to extrapolate results derived from these Boussinesq equations to atmospheres, they do contain descriptions of many of the processes believed to be of fundamental importance. Scale interactions via nonlinearity, convective driving, and the latitude dependent Coriolis forces are all present. That we now have only a meagre understanding of thermally driven flows described by (2.1) - (2.3) suggests that a laboratory analog of these somewhat simplified equations should be very useful in verifying existing theoretical results and in providing useful scale information for generating further approximations in the solutions of these equations.

It is not altogether obvious that a laboratory analog of (2.1) - (2.3) can be made. The principal difficulty arises in generating the radial buoyancy force. We propose to do this in a system which takes advantage of the temperature dependence of the dielectric constant of certain liquids. Consider a dielectric liquid contained in the spherical annulus of Fig. 1. The dielectric constant is

$$\epsilon = \epsilon_o \left[1 - \gamma (T - T_o) \right] \tag{2.4}$$

where ϵ_0 is the ambient dielectric permittivity, T_0 the ambient temperature (about 22°C in the lab) and γ the thermal coefficient of the permittivity. The equations governing this dielectric fluid flow in an imposed electric field $\underset{\sim}{E}(\underset{\sim}{x})$ is, in the laboratory,

$$\rho_o \left[\frac{\partial \underset{\sim}{u}}{\partial t} + \frac{1}{2} \nabla \underset{\sim}{u} \cdot \underset{\sim}{u} + (\nabla \times \underset{\sim}{u}) \times \underset{\sim}{u} + 2 \underset{\sim}{\Omega} \times \underset{\sim}{u} \right] =$$

$$- \nabla p + g \alpha \rho_o T \hat{z} - \rho \underset{\sim}{\Omega} \times \underset{\sim}{\Omega} \times \underset{\sim}{r} + \nu \nabla^2 \underset{\sim}{u}$$

$$- \frac{E^2}{2} \nabla \epsilon \,, \tag{2.5}$$

$$\frac{\partial T}{\partial t} + (\underset{\sim}{u} \cdot \nabla) T - k \nabla^2 T = \Phi$$

$$- \frac{\epsilon_o \gamma T}{\rho_o c_p} \underset{\sim}{E} \cdot \frac{\partial \underset{\sim}{E}}{\partial t} \quad - \frac{\epsilon_o}{2} \frac{\gamma T (\underset{\sim}{u} \cdot \nabla) E^2}{\rho_o c_p} \,, \tag{2.6}$$

$$\nabla \cdot \underset{\sim}{u} = 0 \,, \tag{2.7}$$

where c_p is the heat capacity of the dielectric liquid and z the direction of the earth's gravitational acceleration. Φ represents viscous heating which is neglected. Now note that if the dielectric heating terms are small enough, and if we can construct a situation where

$$g\rho_0\alpha T\hat{z} - \frac{E^2}{2}\nabla\epsilon \approx T\nabla f(r) \quad ,$$

then the laboratory model will be an analog of the Boussinesq equations on a rotating sphere with radial gravity.

Table II lists properties of a typical silicone oil.

Table II

Properties of Dow Corning 200 fluid

ν	.01 cm^2/sec	10^{-6} m^2/sec
κ	6.4×10^{-4} cm^2/sec	6.4×10^{-8} m^2/sec
α	1.17×10^{-3} $°C^{-1}$	1.17×10^{-3} $°C^{-1}$
ρ_0	.873 grm/cm^3	873 kg/m^3
γ	1.0×10^{-3} $°C^{-1}$	1.0×10^{-3} $°C^{-1}$
c_p	.45 cal/grm °C	1.9×10^3 j/kg °C

This fluid has a Prandtl number $P_r = \nu/\kappa = 15$.

For various reasons we will be setting up an ac electric field between the conducting boundaries of the spherical annulus. The frequency ω of the field will be constant and much greater than that of the thermally driven fluid motions whose time scale

will be on the order of the rotation period or the advective time scale, whichever is smaller. The motion frequency will be less than 1/sec. Over these time scales of 1 second or larger the first thermoelectric term in (2.6) has zero average and can be neglected. The second has magnitude

$$\frac{\epsilon_o \gamma T E^2 d^2}{\kappa \rho C_p (T_i - T_o)} \left(\frac{v}{d} = 1/s \right)$$

relative to the conduction term. For an applied temperature difference of 2 C, a field of 10^6 V/m, and a 1 cm gap, this ratio is 10^{-2} or less. If the dielectric fluid is lossy an internal heat generation term of form $\epsilon_o E^2 \omega L / \rho C_p$ should be added to the left hand side of (2.6). For silicone oil the loss factor L is so low that this term is of order 10^{-5} with respect to the conduction term. The fluid resistivity is so high as well (10^{16} ohm/cm) that the Joule heating is infinitesimal. Thus to an excellent approximation the thermodynamics in this laboratory situation ore essentially identical to that in the original Bousinesq model where only diffusion, advection, and time changes of temperature were considered.

Now let us look at the momentum equations. We have neglected free charge forces $\sigma_f \underset{\rightarrow}{E}$. If the driving field frequence ω is much greater than the relaxation frequency ~ ($\epsilon \cdot$ resistivity)$^{-1}$ ~ 10^{-2}sec this force is negligible. This is why we must drive with an ac field with frequency $\gtrsim$ 60 hz. Consider the forcing terms we are retaining, namely

$$\underset{\rightarrow}{f} \equiv -\nabla P + g \rho_o \alpha T \nabla z + \epsilon_o E^2 \gamma \nabla T / 2$$

appearing on the right hand side of (2.5). In a divergence-free fluid

with no-slip boundary conditions the dynamics are determined by vorticity equations obtained by taking the curl of (2.5) and (2.1). The vorticity equations will be identical except for differences in curl $\underset{\rightarrow}{f}$. We have

$$curl\, \underset{\rightarrow}{f} = g\rho_0 \alpha \nabla T \times \nabla z + \frac{\epsilon_0 \gamma}{2} \nabla E^2 \times \nabla T \,. \tag{2.8}$$

Thus if $E^2 = E^2(r)$ and the background gravitational acceleration is small, the system of equations (2.5) is equivalent to (2.1) where the original $\rho_0 g(r)\alpha\nabla r$ in (2.1) is replaced by $\frac{\epsilon_0 \beta}{2} \nabla E^2(r)$.

We can look at this another way. Since the boundary conditions don't involve the pressure we can rewrite a new composite pressure

$$P_m \equiv P - \epsilon_0 E^2(r) \gamma T / 2 \,.$$

Now

$$\underset{\rightarrow}{f} = -\nabla P_m + g\rho_0 \alpha T \nabla z - \frac{\epsilon_0 \gamma T}{2} \nabla E^2(r)$$

$$= -\nabla P_m + T(\phi_l + \phi_e),$$

where ϕ_l is the laboratory geopotential

$$\phi_l = g\rho_0 \alpha z$$

and ϕ_e the equivalent electromagnetic geopotential,

$$-\epsilon_0 \gamma E^2(r)/2 \,.$$

Thus the primitive equations are equivalent since on an astronomical body $\phi = \alpha\rho_0 G(r)$.

Experimentally we impose an alternating electric potential ψ between inner and outer shells. We can ground the inner shell and apply $\psi = V \sin\omega t$ to the outer shell. The average potential ψ in the liquid is then

$$\psi = \frac{R_o}{R_i - R_o}\left(\frac{R_i}{r} - 1\right) .$$

Using this we can compute the ratio of the terrestrial buoyancy force f_t to the electrodynamical buoyancy force f_m. We have

$$\frac{f_m}{f_t} \doteq 64 \epsilon_o \gamma \left(\frac{R_i R_o}{R_o - R_i}\right)^2 V^2 / \{ g \alpha \rho_o (R_i + R_o)^5 \} . \quad (2.9)$$

This equation shows the need to make $R_o - R_i$ and R_i itself small. We would like to make f_m/f_t very large so that the buoyancy force will be effectively radial. For R_i = 2 cm, R_o = 3 cm,

$$\frac{f_m}{f_t} \doteq .002 \, (V_{kv})^2 / g$$

using fluid data from Table II. Clearly large fields O(50kv) are necessary if f_m/f_t is to be large in the terrestrial laboratory where $g \sim 10$ m/sec^2. Unfortunately dielectric fluids tend to be electrically unstable at these fields. However in an orbiting laboratory with $g \sim .001$ m/sec^2 a 2.5 kv field gives a f_m/f_t ratio of 12.

Further discussion is facilitated if we nondimensionalize our equations using the scales κ/d for velocity ($d = R_o - R_i$), d^2/κ for time, ΔT for temperature (ΔT might be the difference between inner and outer

applied wall temperature) and κ^2/d^2 for pressure. These scales are substituted into (2.5) - (2.7) after the thermoelectric terms in (2.6) and the centrifugal terms in (2.5) have been dropped. This latter action is consistent for laboratory flows where

$$F_r \equiv \frac{\Omega^2 R_i}{g} \ll 1$$

With $g \gtrsim 1$ m/sec^2 (the electrodynamic "accelerator"), $R_i \sim .01$ m, this condition implies that $\Omega \ll 10$ rad/sec. We will be concerned with models where $\Omega \sim 1$ so F_r will be small.

We define the characteristic dimensionless parameters of this problem:

$$R_a = \text{Rayleigh number} = \frac{g_o \alpha \Delta T d^3}{\kappa \nu} > 0 \qquad (2.10)$$

$$P_r = \text{Prandtl number} = \nu/\kappa \qquad (2.11)$$

$$T_a = \text{Taylor number} = \frac{4\Omega^2 d^4}{\nu^2} \qquad (2.12)$$

$$\beta = R_i/d \qquad (2.13)$$

If π is the electrodynamically modified dimensionless pressure, the governing equations are:

$$\frac{\partial \underset{\rightarrow}{u}}{\partial t} + \frac{1}{2}\nabla \underset{\rightarrow}{u}^2 + (\nabla \times \underset{\rightarrow}{u}) \times \underset{\rightarrow}{u} + P_r T_a^{1/2} (\hat{z} \times \underset{\rightarrow}{u})$$

$$= -\nabla \pi + P_r (\nabla^2 \underset{\rightarrow}{v} + \cdots)$$

$$+ R_a P_r T \hat{z}/\chi + \frac{(1+\beta)^5}{r^5} R_a P_r T \hat{r}, \qquad (2.14)$$

$$\frac{dT}{dt} = \nabla^2 T \tag{2.15}$$

$$\nabla \cdot \underset{\rightarrow}{u} = 0 . \tag{2.16}$$

In the above equations g_0 is the electrodynamic acceleration

$$g_0 \equiv 2\epsilon_0 \gamma V^2 \beta^2 / \rho_0 \alpha d^3 (1+\beta)^3 \sim .003\ V_{kv}^2\ (m/sec^2)$$

and

$$\chi \equiv g_0/g .^{*}$$

In the terrestrial laboratory $\chi \sim .02$ at 8 kv, in orbiting laboratory $\chi \sim 20$ at the same voltage. Thus we see the great advantage (or even necessity) of doing these experiments in space. Suppose the boundary conditions at $r = \beta, \beta + 1$ (inside and outside shells) are

$$u = v = w = 0$$

$$T(\beta) = \beta + 1$$

$$T(\beta + 1) = \beta. \quad (\text{note } \Delta T = T(\beta + 1) - T(\beta) = -1)$$

Then $T = +\beta(\beta + 1)/r$, $\underset{\rightarrow}{u} = 0$, $\pi \propto R_a P_r / r^5$ solve the basic equations when $\chi \to \infty$. This basic state of no motion and radial (unstable) temperature gradient can be superimposed onto the field variables. In spherical polar coordinates the equations with u, v, w being the east (Θ), north ($+\phi$) and radial velocities respectively are:

$$\frac{\partial u}{\partial t} + \underset{\rightarrow}{u} \cdot \nabla u + \frac{uw}{r} - \frac{uv}{r} \tan\phi = -\frac{1}{r\cos\phi} \frac{\partial \pi}{\partial \theta} \tag{2.17}$$

$$- P_r T_a^{1/2} w \cos\phi + P_r T_a^{1/2} v \sin\phi + P_r \zeta \nabla^2 u$$

* Numerical values computed with R_i=2cm, d=1cm, and fluid data from Table II.

$$+\frac{2}{r^2\cos\phi}\frac{\partial w}{\partial\theta}-\frac{2\sin\phi}{r^2\cos^2\phi}\frac{\partial v}{\partial\theta}-\frac{u}{r^2\cos^2\phi}\Big\}\,,$$

$$\frac{\partial v}{\partial t}+\underset{\rightarrow}{u}\cdot\nabla v+\frac{vw}{r}+\frac{u^2\tan\phi}{r}=-\frac{1}{r}\frac{\partial\pi}{\partial\phi}-P_r T_a^{1/2}\sin\phi\, u$$

$$+P_r\Big\{\nabla^2 v+\frac{2}{r^2}\frac{\partial w}{\partial\phi}-\frac{v}{r^2\sin\phi}-\frac{2\cos\phi}{r^2\sin^2\phi}\frac{\partial u}{\partial\theta}\Big\} \qquad (2.18)$$

$$+R_a P_r T\cos\phi/\chi+R_a P_r\beta(\beta+1)\cos\phi/r\chi\,,$$

$$\frac{\partial w}{\partial t}+\underset{\rightarrow}{u}\cdot\nabla w-\frac{u^2}{r}-\frac{v^2}{r}=-\frac{\partial\pi}{\partial r}+P_r T_a^{1/2}\cos\phi\, u$$

$$+P_r\Big\{\nabla^2 w-\frac{2w}{r^2}-\frac{2}{r^2\cos\phi}\frac{\partial v\cos\phi}{\partial\phi}-\frac{2}{r^2\sin\phi}\frac{\partial u}{\partial\theta}\Big\} \qquad (2.19)$$

$$+\frac{(1+\beta)^5}{r^5}R_a P_r T+R_a P_r\sin\phi\, T/\chi+R_a P_r\sin\phi\,\beta(\beta+1)/r\chi\,,$$

$$\frac{\partial T}{\partial t}+\underset{\rightarrow}{u}\cdot\nabla T=\beta(1+\beta)\frac{w}{r^2}+\nabla^2 T\,, \qquad (2.20)$$

$$\frac{1}{r^2}\frac{\partial r^2 w}{\partial r}+\frac{1}{r\cos\phi}\frac{\partial}{\partial\phi}v\cos\phi+\frac{1}{r\cos\phi}\frac{\partial u}{\partial\theta}=0\,, \qquad (2.21)$$

where

$$\underset{\rightarrow}{u}\cdot\nabla=w\frac{\partial}{\partial r}+\frac{v}{r}\frac{\partial}{\partial\phi}+\frac{u}{r\cos\phi}\frac{\partial}{\partial\theta}\,.$$

3. Comments on the electrohydrodynamics

In the previous section we showed that for large values of χ the thermally driven motion of a dielectric fluid in a spherical capacitor is described by the same equations as that of a thermally driven rotating shallow atmosphere or reasonably deep ocean on a spherical planet, when the small scale motions for the latter are modelled by constant eddy viscosity. Several assumptions were made in the representation of the electrohydrodynamical effects in the fluid which were important in obtaining the desired result that a radial gravity field could be simulated. Although the subject of electrohydrodynamics is a relatively new field there have been several previous studies which lend support to the assumptions used here.

As mentioned above, there are several surface instabilities related to surface electrical stresses on a dielectric liquid with a free surface. These are discussed in the review by Melcher and Taylor (1969). Suffice it to say that they have no geophysical analogs and are undesirable in our model experiment. They are eliminated by applying rigid electrically conducting boundary conditions to the fluid. Since this is the natural configuration for our spherical capacitor we will have no trouble with the surface modes of instability.

Among the bulk fluid instabilities possible when the dielectric fluid is subject to both thermal and electric fields are (a) the electrohydrodynamic Rayleigh-Taylor instability that we desire in our study of solar

and planetary convection and (b) an instability related to free-charge effects Turnbull(1971a). We have assumed that instability (b) can be eliminated by applying an ac field of high enough frequency. Turnbull and Melcher (1969) and Turnbull (1970) have shown by comparing theoretical and experimental results that the Rayleigh-Taylor instability in a plane layer of fluid between horizontal conducting surfaces behaves as described by the Boussinesq equations neglecting thermoelectric and free-charge effects. In their experiments the gradients of E are small and related to the weak temperature dependence of ε (e.g., $\nabla \cdot \underline{D} = 0$ yields an $\underline{E}$ with gradients of order $\gamma\Delta T$). In our experiments a strong E gradient is imposed geometrically so that free charge effects will be relatively weaker in comparison with polarization force effects. Their experiments were done using a silicone fluid quite similar to the one we propose to use and the good agreement they achieve encourages us that we are properly representing the electrohydrodynamics. A similar study of the effect of a non-uniform alternating electric field on a thermal boundary layer was reported by Turnbull (1971b) and this too gives us confidence in the reduced equations (2.14) - (2.16). Further supportive evidence comes from the study of Chandra and Smylie (1972) who show that the convective instability of a differentially heated dielectric fluid in an alternating axially symmetric field occurs at the predicted critical Rayleigh number computed using equations like (2.14) - (2.16) with $\chi \to \infty$ as a starting point.

Based on these studies we have reasonable confidence that the electrohydrodynamical behavior of the silicone fluid at moderate temperature differences and large 60 hz fields is described by our model equations. It remains to verify this for our particular geometry. This is largely a question of how to get adequate data. We discuss this in following sections. Note however that we have also assumed that $\underset{\rightarrow}{E}$ is a function of r only. In a perfect spherical capacitor this is obvious, but in a real experiment we need to have a feedthrough tube to maintain the inner sphere at constant voltage and temperature. Near the "neck" then $\underset{\rightarrow}{E} = \underset{\rightarrow}{E}(r, \phi)$ and the term $\nabla E \times \nabla T$ will not be zero for the basic state $T(r) = -\beta(1+\beta)r$ as it should be. Thus we must conduct our experiment far enough away from the neck so that $\underset{\rightarrow}{E}$ is primarily radial. This is accomplished by performing experiments only in the upper hemisphere opposite the feedthrough. The lower hemisphere is isolated by a radial plastic disc at the equator. For small but reasonable neck sizes and $\beta \gtrsim 3$ the field, as calculated by numerical solution of Laplace's equation, will be about 95% radial in the entire upper hemisphere. Note that the lower voltages required when the experiment is run in a low g environment means that the neck can be substantially smaller than that needed for insulation in the terrestrial laboratory. Thus it is probable that in the zero g environment more than a hemisphere could be studied.

4. Geophysically relevant parameter ranges

To discuss what values of R_a, T_a, β and P_r would be most interesting to use in the experiments requires an appreciation of what astro-geophysical problems are important. A complete review of what is known about convection in a rotating spherical shell and of what we would like to know is beyond the scope of this report. Let us briefly look at the conceptually simplest case of uniformly heated smooth surfaces to illustrate the kinds of questions we can hope to answer with this experiment. Obviously, more complicated thermal boundary conditions and surface irregularities could be included and studied experimentally. The types of problems are perhaps obvious to meteorologists and oceanographers. The questions arising in the study of non-linear mechanics are similar in a wide manifold of problems so we will focus on the simplest forced problem--one which is by no means well understood.

The uniformly, unstably heated, rotating spherical shell of fluid serves as a model problem for large scale planetary and solar convection. The principle motivation for this model comes from observations of large scale giant convective cells on the sun and (possibly convective) axisymmetric rings at low latitudes and cells at high latitude on Jupiter. The study of this problem has by and large followed that of convection in a plane non-rotating fluid layer. In particular we would like to understand the mechanism for planform selection. In the plane layer the preference for two-dimensional rolls or three-dimensional hexagons is

related to calculable non-linear stability properties. In the spherical rotating shell the calculations are by no means as simple partly because with the latitude variation of Coriolis force the global linear problem is non-separable in the horizontal coordinate. Under different external constraints (rotation, viscosity, etc.) it is theoretically possible for the linear convective instability to consist of banana cells (Busse, 1970) extending from pole to pole, axisymmetric zones or belts (Williams and Robinson, 1973) or various forms in between (Gilman, 1972). In all these theoretical studies, convection first occurs as weak motions, superimposed in the background state of unstable temperature gradient and no motion when R_a exceeds some critical value R_{ac} (T_a, β, P_r). In plane non-rotating convection with rigid conducting boundaries $R_{ac} = 1708$. Gilman (1972) has determined R_{ac} for the equatorial annulus. The computations, which are quite time consuming, show that R_a increases monotonically with T_a from about 700 at $T_a = 0$ to 10^4 at $T_a = 10^6$. Clearly, since we want to study convection, our experimental values of R_a must exceed these numbers.

The non-linear processes are of most interest since R_a is very much greater than R_{ac} for solar and planetary atmospheres. The appropriate values of R_a for the astronomical cases are not easy to estimate because of poor knowledge of the eddy viscosity ν and the depth d. Clearly the R_a appropriate for the large scale convection is very large. For the sun $R_a \sim 10^2 R_{ac}$, using $d = 10^{10}$cm, $\nu = 3 \times 10^{13}$, $\kappa \sim \nu$, and $g\Delta T/T_o = 10^2$.

This represents little more than a best guess. It is clear however that the cases of most interest in astrophysical problems are those for which R_a is many times critical. These values are easily attained in the experiment.

As R_a increases above R_{ac} several interesting questions emerge. How long do the linear modes persist? Do the orientations of planforms suggested by linear theory persist, or do they become unstable and get replaced by a new planform? This is of particular importance in Williams and Robinson's (1973) model of Jupiter's cloud bands since they got axisymmetric bands by setting $\frac{\partial}{\partial\theta} = 0$ in their equations! They did make a numerical stability analysis of their axisymmetric solutions but due to the enormous computation time required this aspect of the problem is by no means solved. In our experiments we should be able to observe the preferred cells' shapes and orientations as a function of $R_a - R_{ac}$, T_a, P_r and β.

As the convective flow field becomes moderately non-linear $(R_a - R_{ac})/R_{ac} \gtrsim 1$, the "simple" modes of linear theory will interact with themselves and other modes to produce a spectrum of disturbances and perhaps to generate a mean axisymmetric flow. The question of what kind of mean flow the convection cells can produce is of great importance in view of the observed equatorial accelerations on the sun and the giant planets. Numerical models (Gilman, 1973) for relatively small $(R_a - R_{ac})/R_{ac}$ have shown the tendency to generate mean flows. Being three-dimensional and time dependent such models are complicated and cannot handle too

wide a spectrum of disturbance (hence they are confined to moderate non-linearity). The laboratory experiment should be able to verify these moderately non-linear results and provide information on wave-wave interaction which will hopefully provide data for realistic theoretical approximation. In addition measurements should be made of mean-flows generated at strongly non-linear conditions (large $R_a - R_{ac}$) which will probably remain inaccessible to numerical experimentation for some time.

In order to ahieve the above goals we must be able to obtain key measurable quantities, a problem discussed below, and have access to the proper parameter range. For a typical experimental set up in a zero g environment we find that R_a can be set from 0 to 10^6 and T_a from 0 to about 4×10^5. Thus one can cover the weakly and strongly unstable limits for both the weak and strong rotation cases. Figure 2 shows a parameter plot of the regions accessible by this experiment on a diagram which also shows the numerically calculated neutral stability curve for large scale convective instability of rotating stratified flow on a sphere (from Gilman, 1972). The experiment can give data on flows which are more strongly non-linear than can currently be handled on a computer or by asymptotic methods. Note also that viscous effects will be confined to lengths of order $d/T_a^{1/4}$ or $d/R_a^{1/4}$ so that in the large (R_a, T_a) regions viscosity will be apparent only in narrow boundary layers.

Figure 2. Typical experimental range for direct electroconvection in a spherical shell with uniformly heated surfaces. The solid curves show the theoretical linear stability curves. The hatched line encloses the parameter values accessible experimentally.

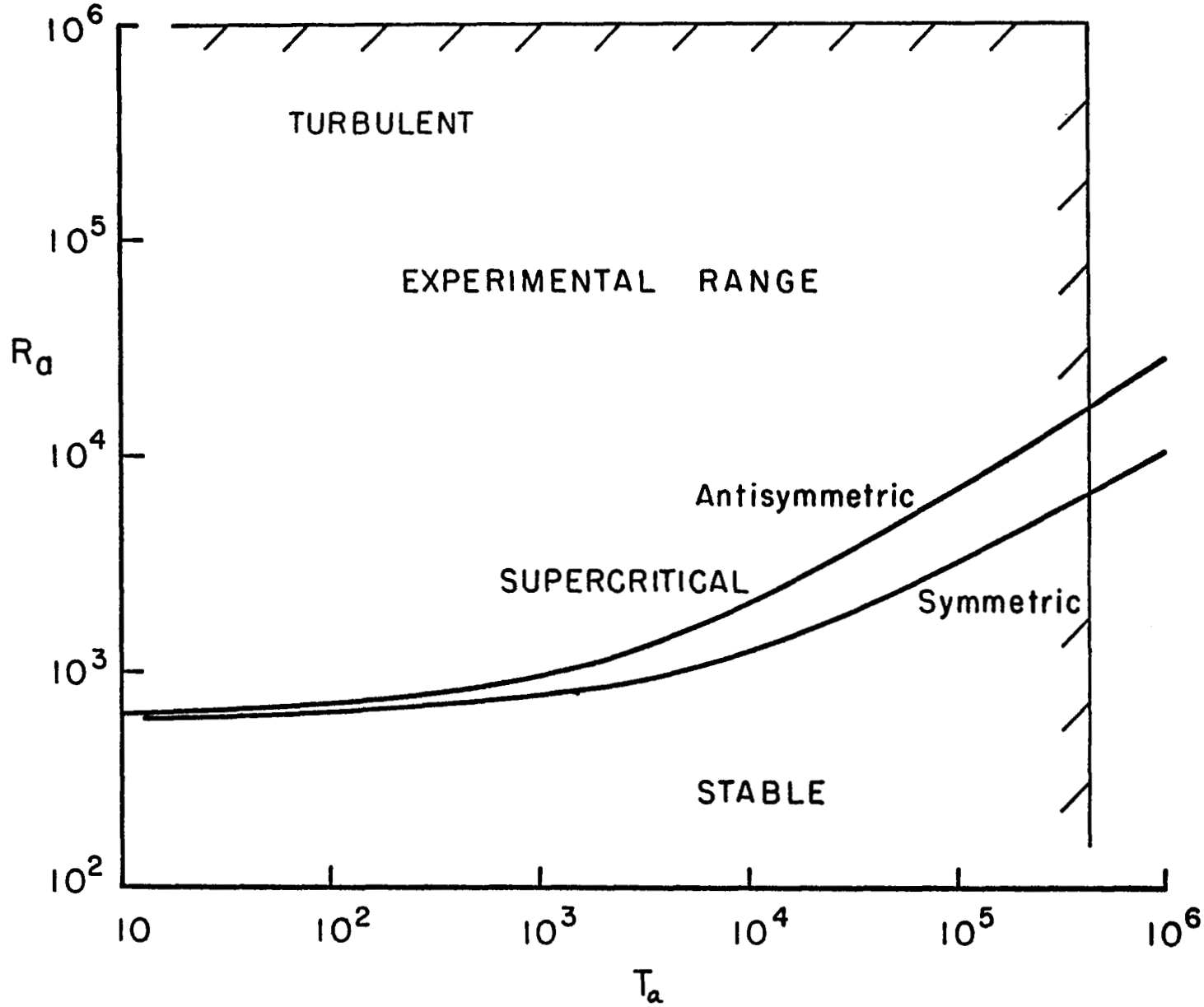

This is only one example. In general we expect to be able to study weak and strong rotational effects in both weakly and strongly non-linear flows. The Prandtl number of the silicone fluids is around 10. Ideally we would like to be able to vary this towards smaller values. This may be possible with other types of fluids.

We view this electro-convection apparatus as a tool for the experimental study of a large number of geophysical flows in which sphericity, stratification, and rotation are all important. There are a wide range of possibilities depending on the kinds of forcing imposed and on the detailed geometry. For example, mechanical driving and the presence of meridional barriers would naturally lead to flows of interest in dynamical oceanography when the stratification is basically stable. Although we have focused on one particular problem, rotating convection, it is obvious that an experimental module in which gravity is effectively radial should have wide applicability.

5. A simple demonstration of electroconvection

We performed a very simple experiment to demonstrate that polarization forces in a stably stratified fluid can overcome the terrestrial gravity. The geometry for this experiment is shown in figure 3. Two horizontal plates at $z = 0$ and $z = a$ are maintained at a temperature difference ΔT. Thus a stable stratification is set up in which there is no motion. Thus any fluid motion or distortion of the stratification away from the form

$$\overline{T} = \frac{\Delta T}{a} z$$

must come from the action of electrodynamic forces alone. This is in contrast to the spherical shell experiments discussed in chapter 6 where there is vorticity generation by buoyancy forces related to earth gravity. Here

$$\nabla\overline{T} \times \nabla\phi_{\ell} = 0 \quad .$$

A thin horizontal rod at $z = z_o$ is maintained at a 60 Hz RMS voltage $V = \Delta V$. The rod is thin enough so that it causes only a minor distortion of the background temperature field. Visualization is achieved by looking through the fluid layer (typically $a \simeq 1$ cm, and the layer is 15 cm wide and deep) at a Moiré fringe pattern oriented vertically. Thermal gradients in the horizontal direction will cause refraction to occur and will cause the apparent position of the fringes to move. For large $\Delta T \simeq 10\,^{\circ}C$ this is a rather sensitive technique and has the advantage that no particles need be placed in the fluid. Particles tend to pick up space charge at large ΔV and dance around. They also tend to settle out under g forces. Thus visualizing the thermal patterns in this way is preferable to particle tracking.

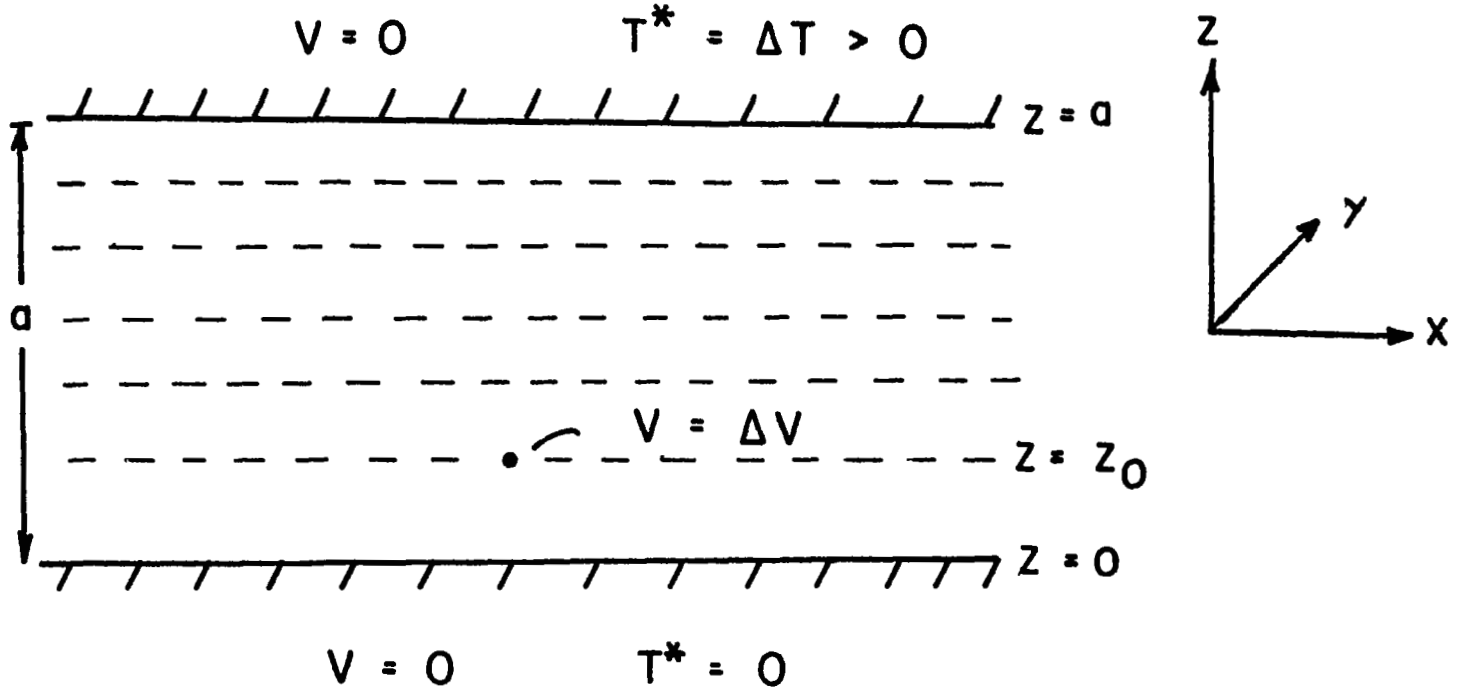

Figure 3. Geometry for the rod experiment. A statically stable thermal stratification is set up by heating the top lid. This is then destabilized by applying a large voltage to a horizontal rod located parallel to the y axis.

Figures 4-7 show the evolution of the fluid state as ΔV is increased. For $\Delta V = 0$ there is only a weak thermal perturbation near the rod. This increases as ΔV is increased. At first the perturbation is primarily thermal. There is a very weak circulation within the elliptical thermal perturbation region of figures 5-6, because weak buoyancy layers are needed near the rod to satisfy the temperature boundary condition there. As ΔV is increased the flow breaks down into unstable plumes near the rod (see Fig. 7). The vertical motions are vigorous and the plumes radiate gravity waves into the stably stratified fluid at large distances from the rod. The upward motion consists of cold fluid rising, and hence is opposite to that generated by the $g \propto T$ term in the vertical equation of motion. Electrohydrodynamic buoyancy forces have overcome the restoring force of terrestrial gravity. 'g' has been reversed.

A formal analysis of this problem is non-trivial. We here indicate a rough theory for the critical value of ΔV needed to generate convection. The potential due to the rod is

$$\phi_{rms} = \frac{\Delta V \ \ln\left\{\dfrac{\sin\frac{\pi}{2a}(z_0 + z + ix)}{\sin\frac{\pi}{2a}(z_0 - z - ix)}\right\}}{\ln\left\{\dfrac{\sin \pi z_0/a}{\pi\rho/2a}\right\}} \qquad (4.1)$$

The diameter of the rod is $\rho << a$. It can be seen that the refractive patterns of Fig. 5 and 6 are strongest near the region of space where ϕ_{rms} is biggest, as we would expect.

Now near the rod

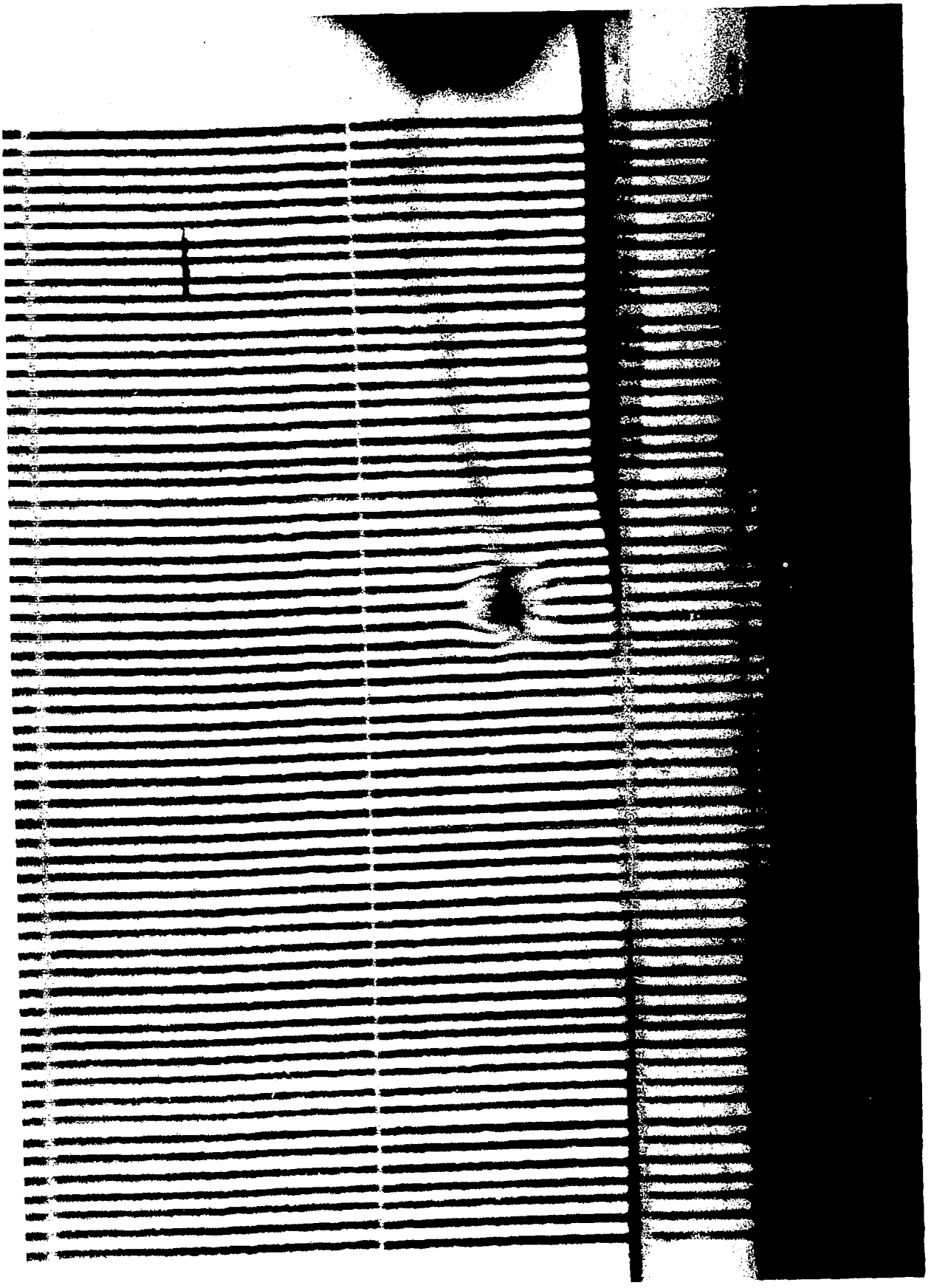

Figure 4. Photograph taken looking through the fluid layer at a series of vertical lines painted on a translucent plastic end wall (at $y = +A$ say, $A \gg a$). The lines 'bend' in response to index of refraction changes in the fluid. Here $\Delta V = 0$ and there is a slight bending near the rod because it is a finite conductor and is not consistent with the static temperature distribution $\overline{T} = \frac{\Delta T}{a} z$. Here $a = 1$ cm, $z_o = 1/2$ cm and $\Delta T = 20°$ C. The fluid is a low viscosity silicone oil.

Figure 5. Same as 4, except ΔV = 2 kv. Note how polarization forces have acted to distort the thermal structure near the rod. There is a very weak recirculating motion near the rod.

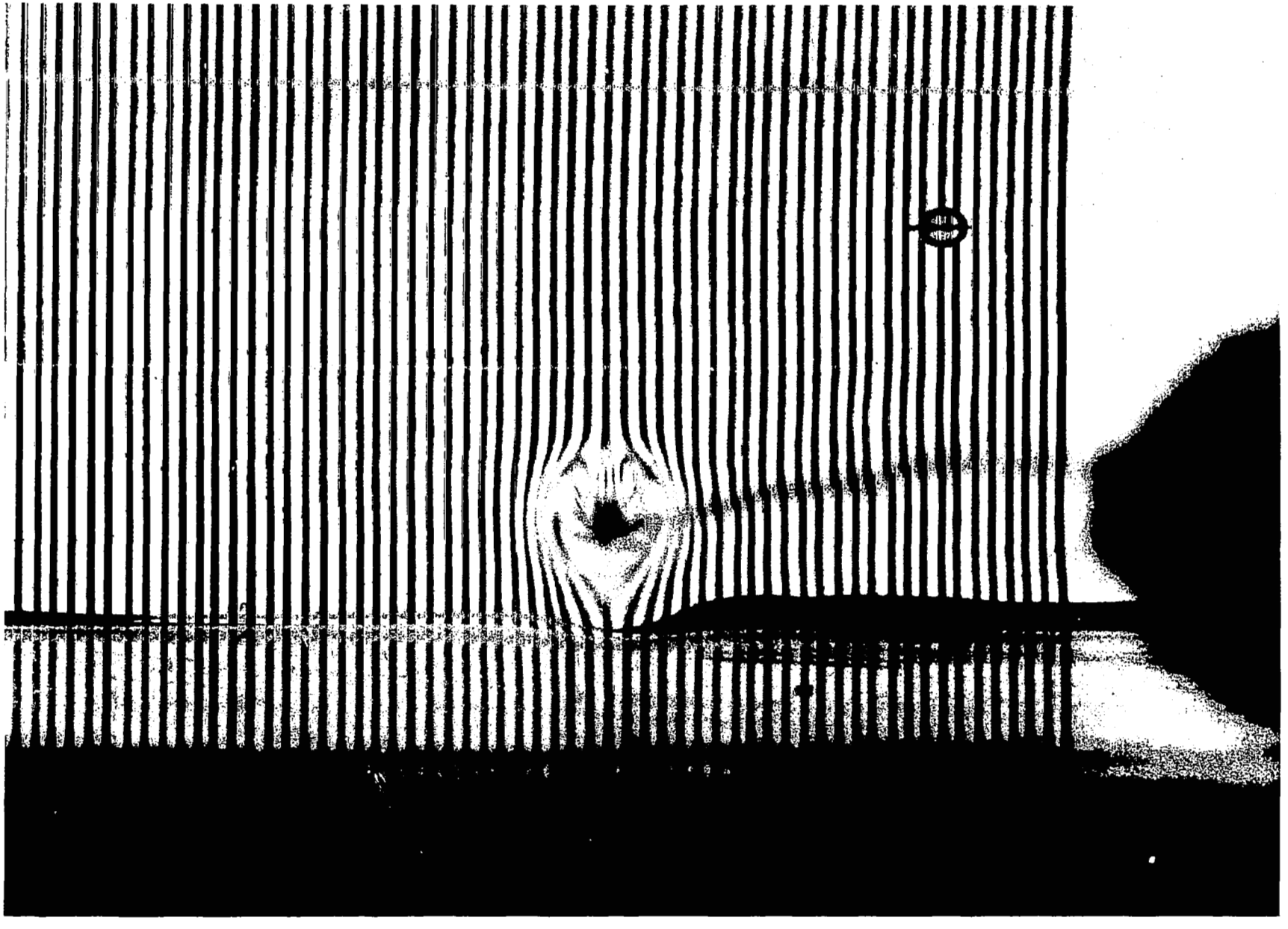

Figure 6. Same as 4, except ΔV = 4 kv. Note increased distortion as polarization forces are strong. Flow is still steady.

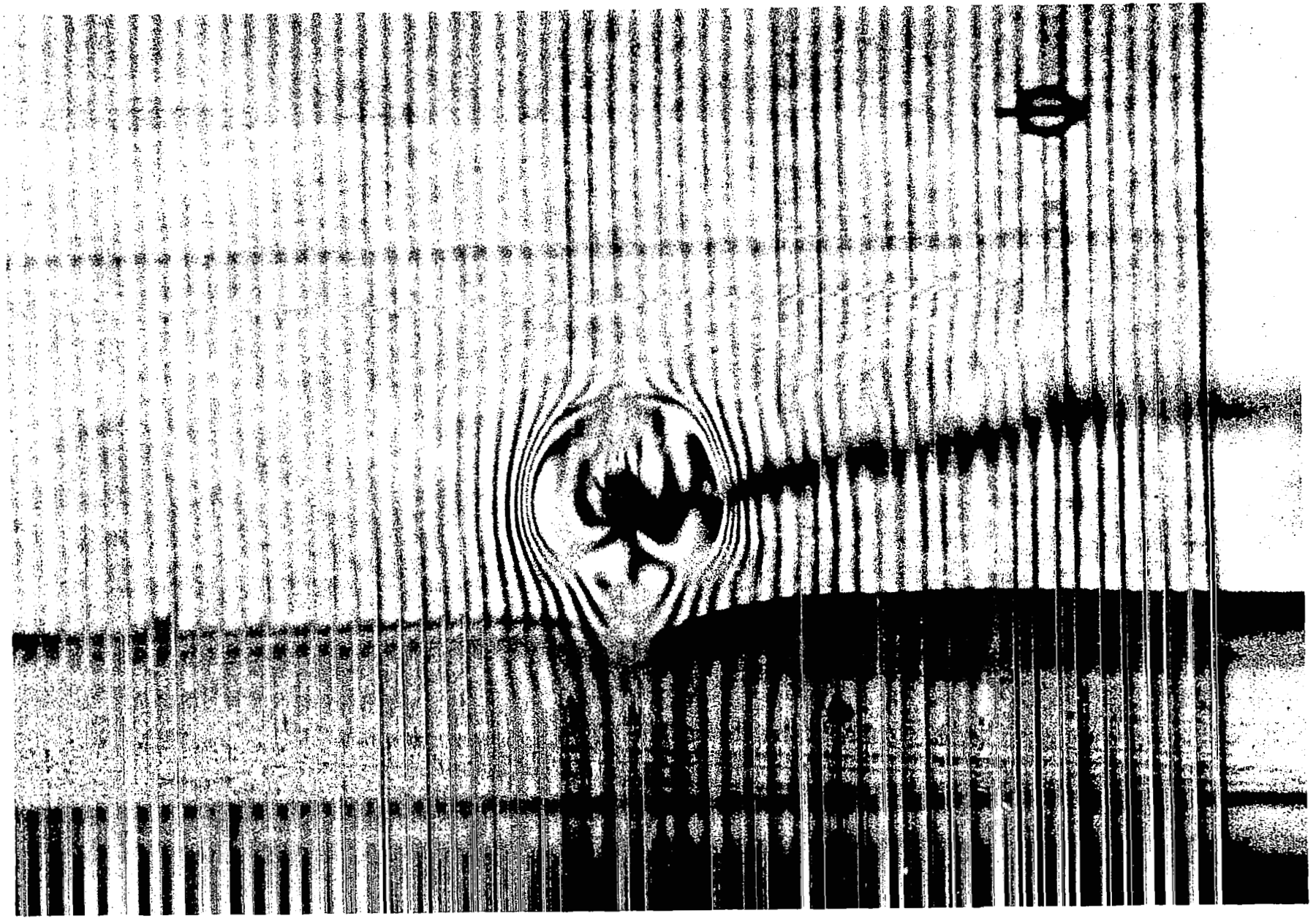

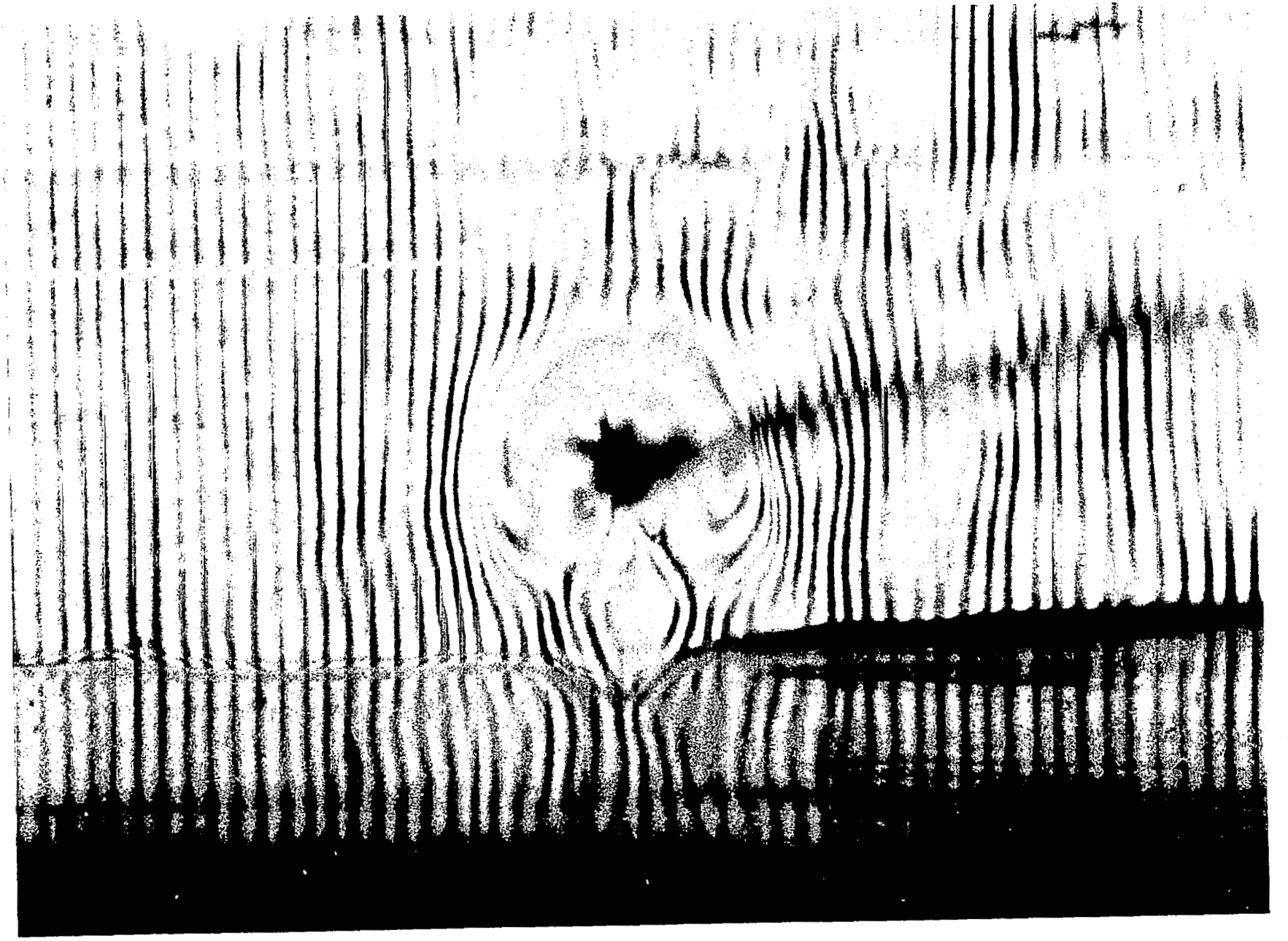

Figure 7. Same as Figure 4, except ΔV = 8 kv. A strong instability has occurred throughout the fluid, with cold fluid rising and hot fluid sinking.

$$E_{\hat{r}}^{*} \equiv -\frac{\partial \phi}{\partial r} = \frac{\Delta V}{\ln\left[\frac{\sin \pi z_0/a}{\pi \rho/2a}\right] r}$$

where r is the radius measured from the rod center. $\rho \leq r << a$. Because of the static stability the motions will be weak (prior to electroconvective instability). If Ψ is the streamfunction for motion in the x-z plane ($w = -\Psi_x$, $u = +\Psi_z$), the equations of steady motion can be combined into the vorticity equation

$$\nabla^4 \psi - R_a T_x + \sigma J(T, E^2) = 0 \qquad (4.2)$$

where T is the thermal departure (dimensionless) from a background temperature, $T_{ambient}$, and $E^2 = 1/r^2$.

$$\sigma \equiv \frac{\Delta V^2 \gamma \epsilon_0 \Delta T}{\ln^2\left\{\frac{\sin \pi z_0/a}{\pi \rho/2a}\right\} \cdot 2 K \nu \rho_0}$$

and

$$R_a \equiv \frac{g \alpha \Delta T a^3}{K \nu}$$

R_a is the normal Rayleigh number based on terrestrial gravity.

Now in this experiment both R_a and σ are very large. Thus the primary balance in (4.2) yields a requirement that there be no net torques

on fluid elements.

Thus writing $T = \overline{T}(z) + T'(x,z)$

$$J(T' + z,\ E^2 - \frac{R_a}{\sigma} z) = 0$$

The solution is

$$T' = \frac{\sigma}{R_a} E^2$$

which is less than 1 for $r > \rho$ and typical values. In principle this T' could be compared with the refractive patterns in fig. 6, for example.

Since $T' \simeq 1/r^2$ it will not satisfy thermal equilibrium demanded by $\nabla^2 T' = 0$. Thus a weak circulation, constrained by the static stability will be set up.

We imagine that the flow will be unstable when "gravity" is inverted, so that vertical excursions of cold fluid will be reinforced. This is essentially an inviscid criterion (valid because R_a and σ are large) equivalent to the zero voltage condition that $\frac{\partial \overline{T}}{\partial z} < 0$. Looking at the coefficient of T_x' in eqn. (4.2) we see that instability will be possible if

$$R_a + \frac{2\sigma \sin\theta}{r^3} < 0$$

where θ is the polar angle. When $\theta = -\pi/2$ instability is most likely. It is possible when

$$\frac{2\epsilon_0 \Delta V^2}{g\rho_0 \ln^2\left[\frac{\sin \pi z_0/a}{\pi\rho/2a}\right]} \cdot \frac{1}{a^3 r^3} > 1$$

Let $P_m = ra = r^*$ and setting $P_m = 2\rho$ we find that for our little experiment

$$\Delta V \simeq 6 \text{ kv}$$

This compares well with the observed transition value of about 7 kv.

Thus we have demonstrated that electrohydrodynamic forces do behave qualitatively as predicted. But more importantly we have shown that flows at large field strengths can be visualized easily and data concerning fluctuation frequencies, wavelengths, and transition points may be obtained from sequential photographs resembling fig. 7.

6. Calculations and experiment on spherical electroconvection.

We have performed several calculations and experiments investigating the thermally driven flow in a hemispherical cap. That is, the spherical annulus of Figure 1 is divided into a hemisphere by a rigid insulating boundary at the equator. Motion in the upper hemisphere is studied. It is driven by cooling the inner surface relative to the outer. Thus $T_i < T_o$. The fluid motion is now in response to both terrestrial gravity, and to electrodynamic forces. When $\Delta V = 0$ there still will be motion because with this distribution of heating

$$\nabla T \times \nabla \phi_\ell \neq 0$$

In all runs $P_r = 126$, $\beta = 2.36$ and $T_a = 0$. We have focused on the meridional circulation during axisymmetric (no variation with longitude) steady flow, so that the velocity vector has only two components

w = radial velocity = $w(r,\phi)$

and v = poleward velocity = $v(r,\phi)$

where ϕ is the 'latitude', zero at the equator.

Our main purpose in doing these experiments was:

a) to see how electrodynamic effects modify the'Hadley' circulation driven by the sideways heating when $\Delta V = 0$;

b) to demonstrate that flow motions can be visualized by particle tracking at modest fields.

The theoretical solutions of the governing non-linear Navier-Stokes equations (2.17 - 2.21) were obtained numerically by P.A. Gilman,

using a modified computer model originally designed to study solar convection (see Gilman, 1972). The results for fixed P_r, T_a, β depend only on R_a and χ. All results of this section will be presented in terms of

$$R_a = \frac{g\alpha\ \Delta T\ d^3}{k\nu}$$

based on terrestrial gravity, the normal Rayleigh number, and ΔV, the applied ac voltage.

The experimental apparatus has a brass inner spherical shell into which is pumped cool fluid from a thermostated bath. Thermal contrasts ΔT range from 1 to 10°C. The outer shell is glass coated on the inside with a transparent conductive coating (Indium oxide, by Perkin Elmer). The whole shell is immersed in an outer bath maintained at temperature T_o. The working fluid is silicone oil (Dow Corning) laced with a small amount of merlescent pigment, a dielectric compound of small platelets that align themselves with the shear or with the electric potential surfaces. Time photographs are taken of particle streaks. From the photographs both flow structure and velocity data can be recovered.

Figures 8 - 10 show the computed meridional circulation for $\Delta V = 0$. It is basically a Hadley circulation of one cell with cold fluid sinking and hot fluid rising up the outer sphere in response to terrestrial gravity acting on hot and cold fluid. As R_a increases velocities increase and the flow becomes more of a boundary layer nature with a tendency towards stagnation near $r = 1/2$, $\phi = 20°$. At $R_a = 11{,}000$ the thermal distribution is nearly conductive except near the equator where there is radial outflow (fig. 11). At large R_a a stable stratification is developing in the interior (fig. 12) with strong radial thermal gradients

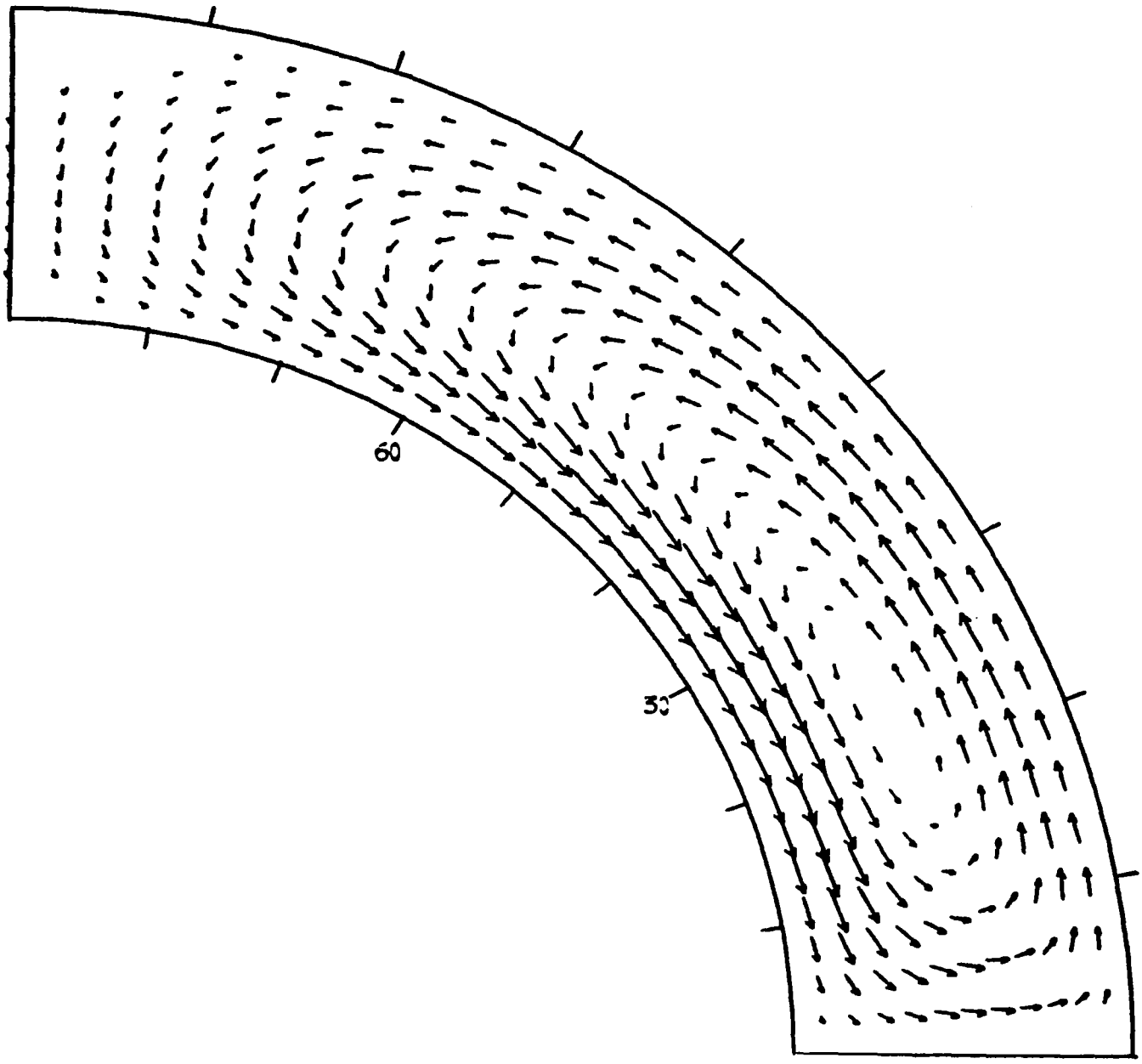

Figure 8. Meridional circulation in a hemispherical shell with $T_a = 0$, $P_r = 126$, $\beta = 2.36$. These parameters are held fixed in all subsequent results. Here $\Delta V = 0$, $R_a = 11{,}000$.

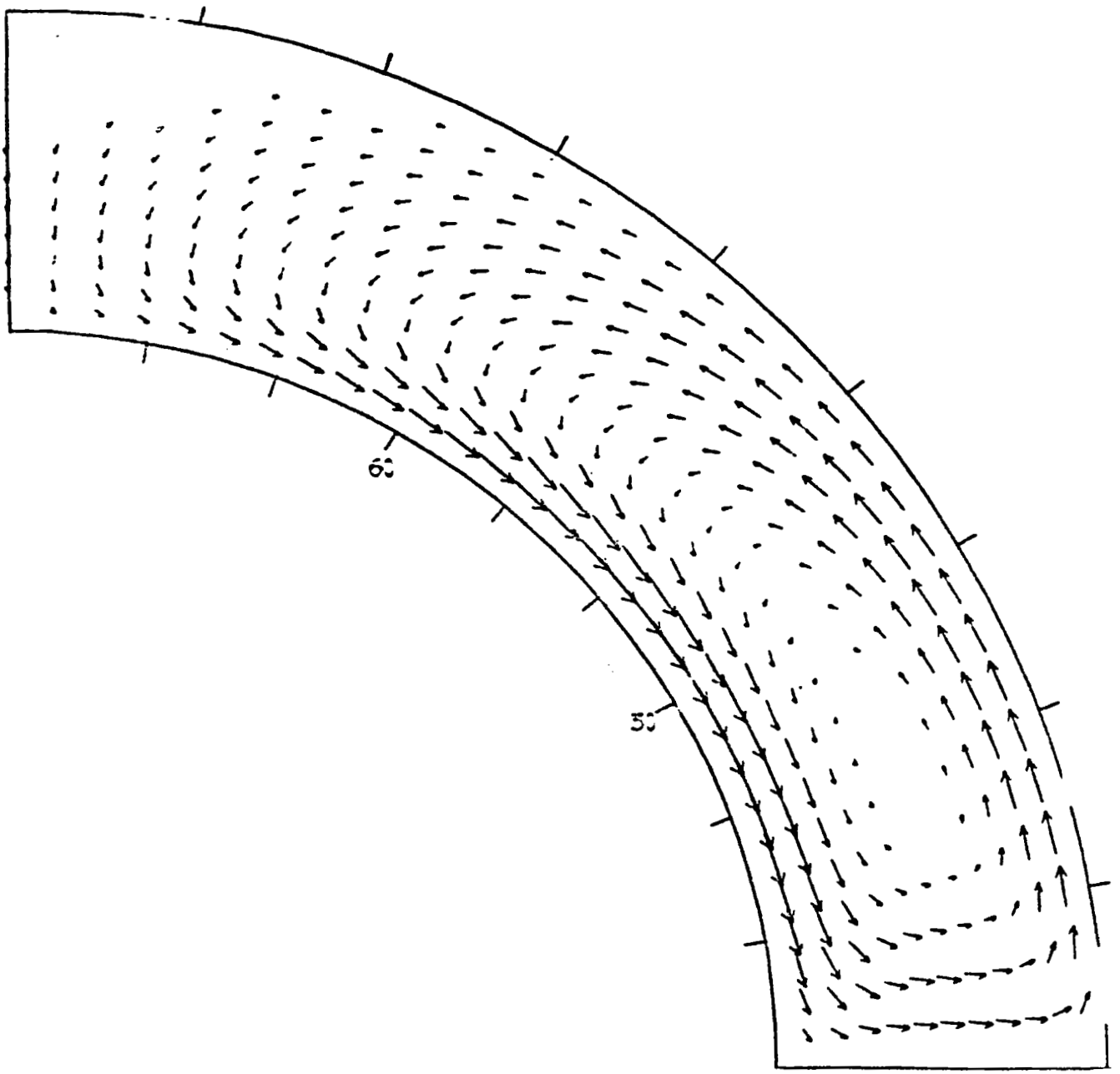

Figure 9. Meridional circulation for $\Delta V = 0$, $R_a = 45{,}000$.

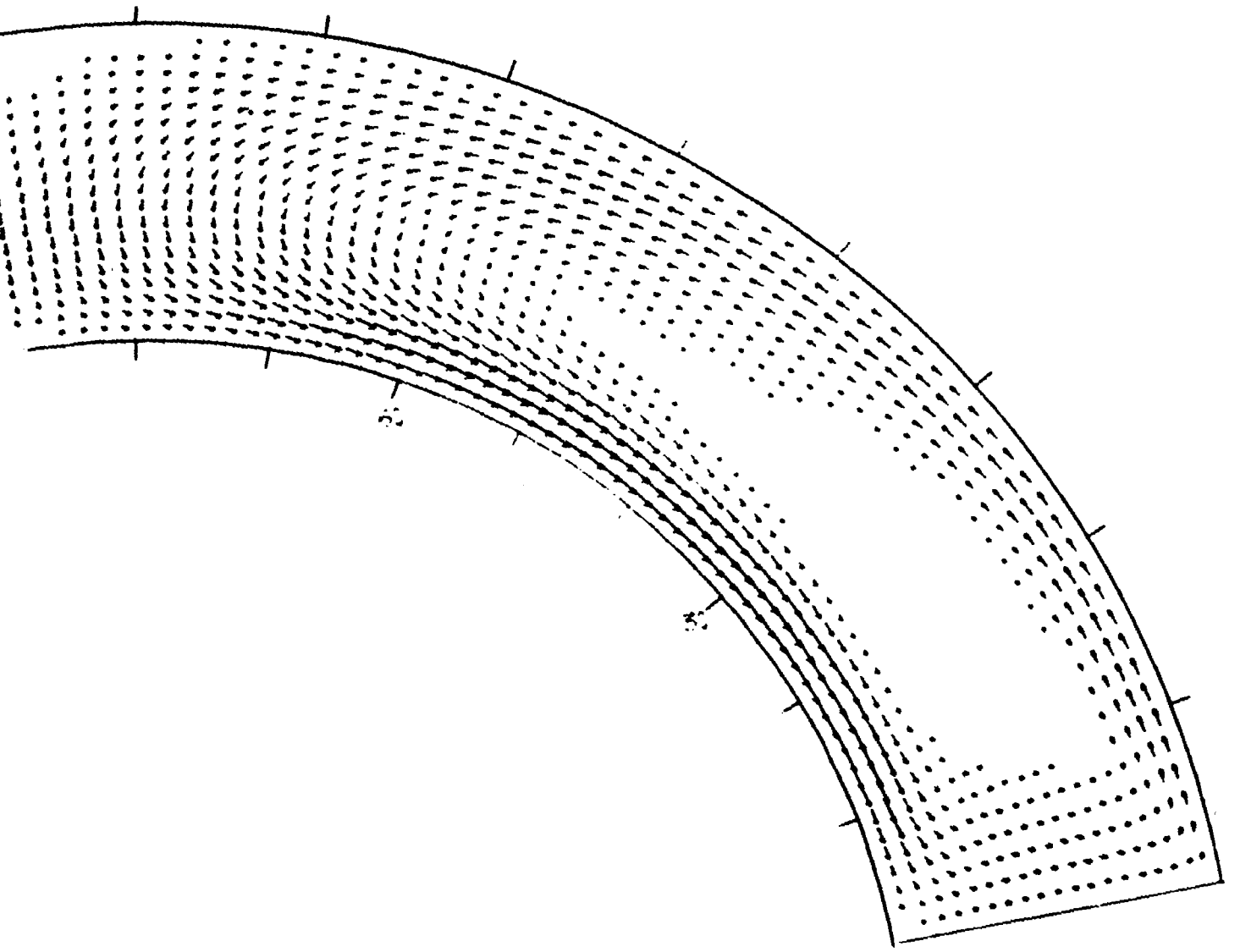

...dional circulation for $\Delta V = 0$, $R_a = 118{,}000.$

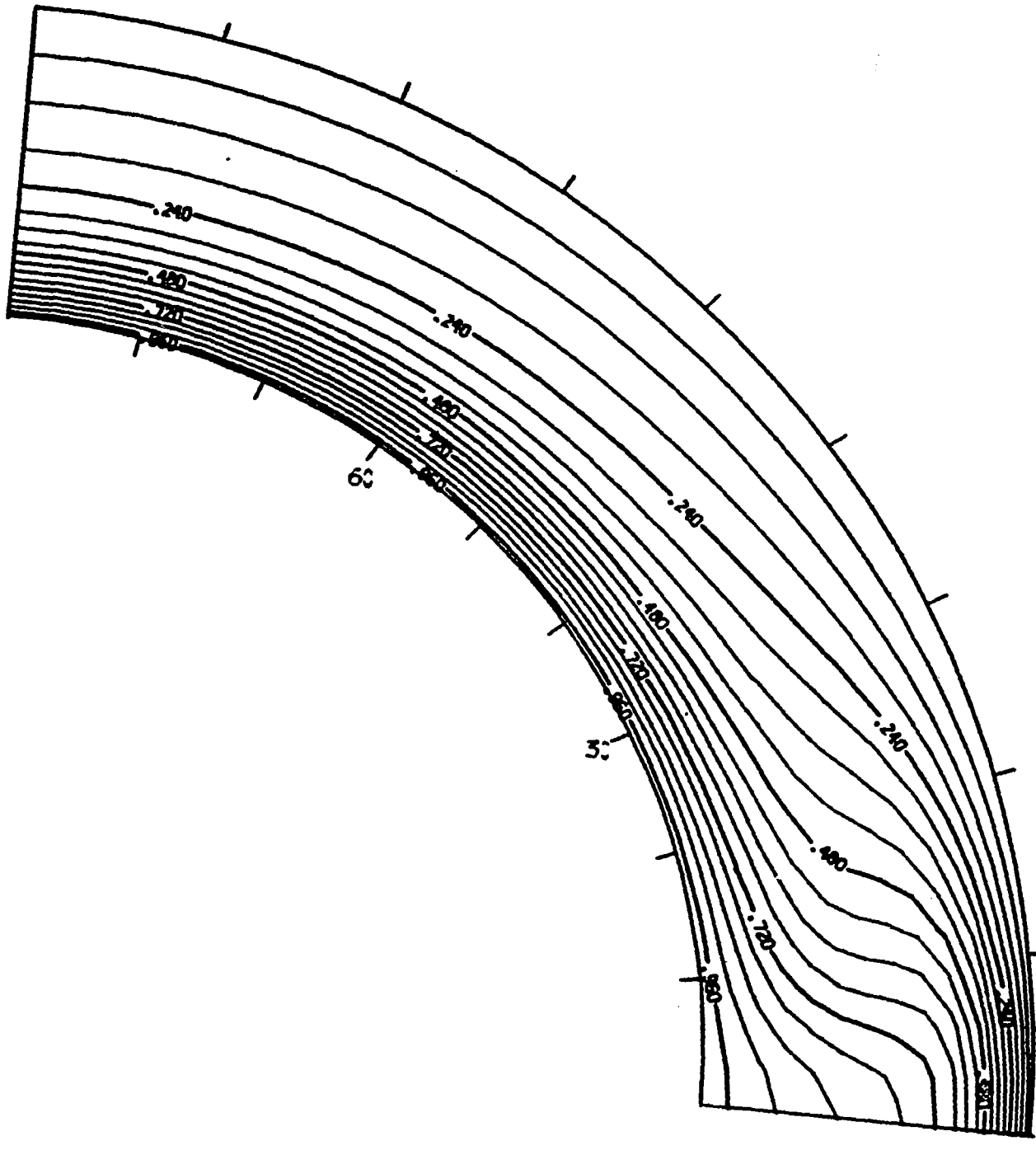

Figure 11. Thermal distribution (scaled by ΔT) for $\Delta V = 0$, $R_a = 11{,}000$.

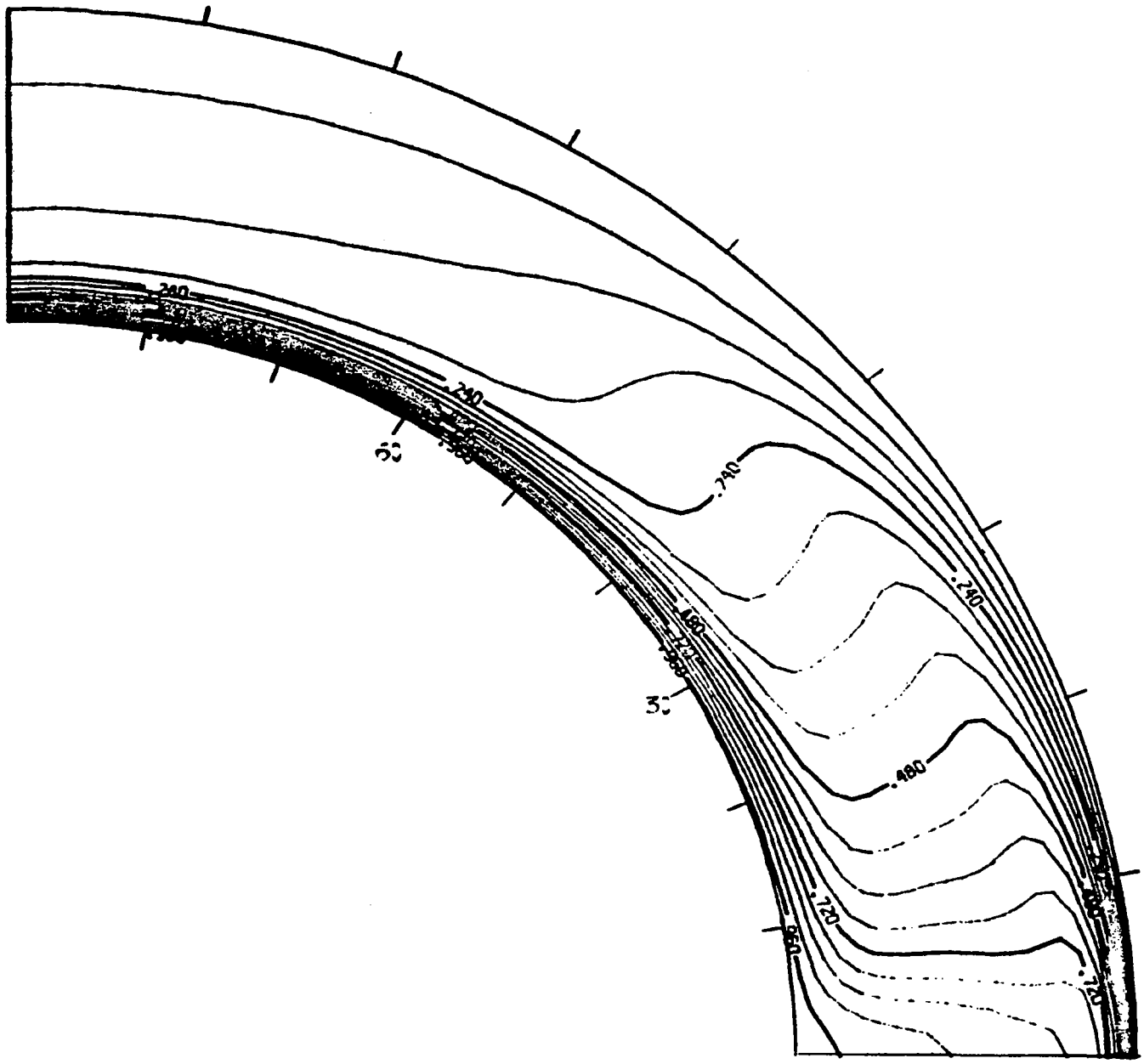

Figure 12. Thermal distribution for R_a = 118,000, ΔV = 0.

only near the walls.

Figs. 13-14 show streak photographs taken by shining a narrow slit of light in towards the vertical axis and positioning the camera at 90° to the slit. The computed and observed circulation patterns are similar. The vacant 'hole' of figure 10 is not really stagnant; the motion is just slower than the cutoff level required for an arrow.

Quantitative comparisons between theory and experiment are shown in figures 15 and 16. The agreement is good. It is very hard to get good data in the high shear regions near the walls because small errors in obtaining the radial position of the particles lead to large errors in the predicted velocities.

Since the agreement was so good for $\Delta V = 0$ we then went on to study electrodynamic effects. However, a problem immediately arose. Fig. 17a and 17b show predicted meridional velocities for two cases. The 15,000 volt case is predicted to be indistinguishable from the zero voltage case. The gravitational Hadley circulation is dominant at these voltages. This is in part a consequence of having weak meridional thermal gradients (i.e. fig. 11). Since electrodynamic forces act via

$$\nabla T \times \nabla E^2(r)$$

and since $\frac{1}{r}\frac{\partial T}{\partial \phi}$ is much less than $\frac{\partial T}{\partial r}$ (recall that $\nabla T \times \nabla \phi_\ell$ has a part $g\alpha \frac{\partial T}{\partial r}\cos\phi$) our original scale analysis of electrodynamic effects vs. gravitational buoyancy effects was an overestimate, in this particular geometric configuration. This problem did not arise in the rod experiment where

$$\nabla T \times \nabla \phi_\ell = 0$$

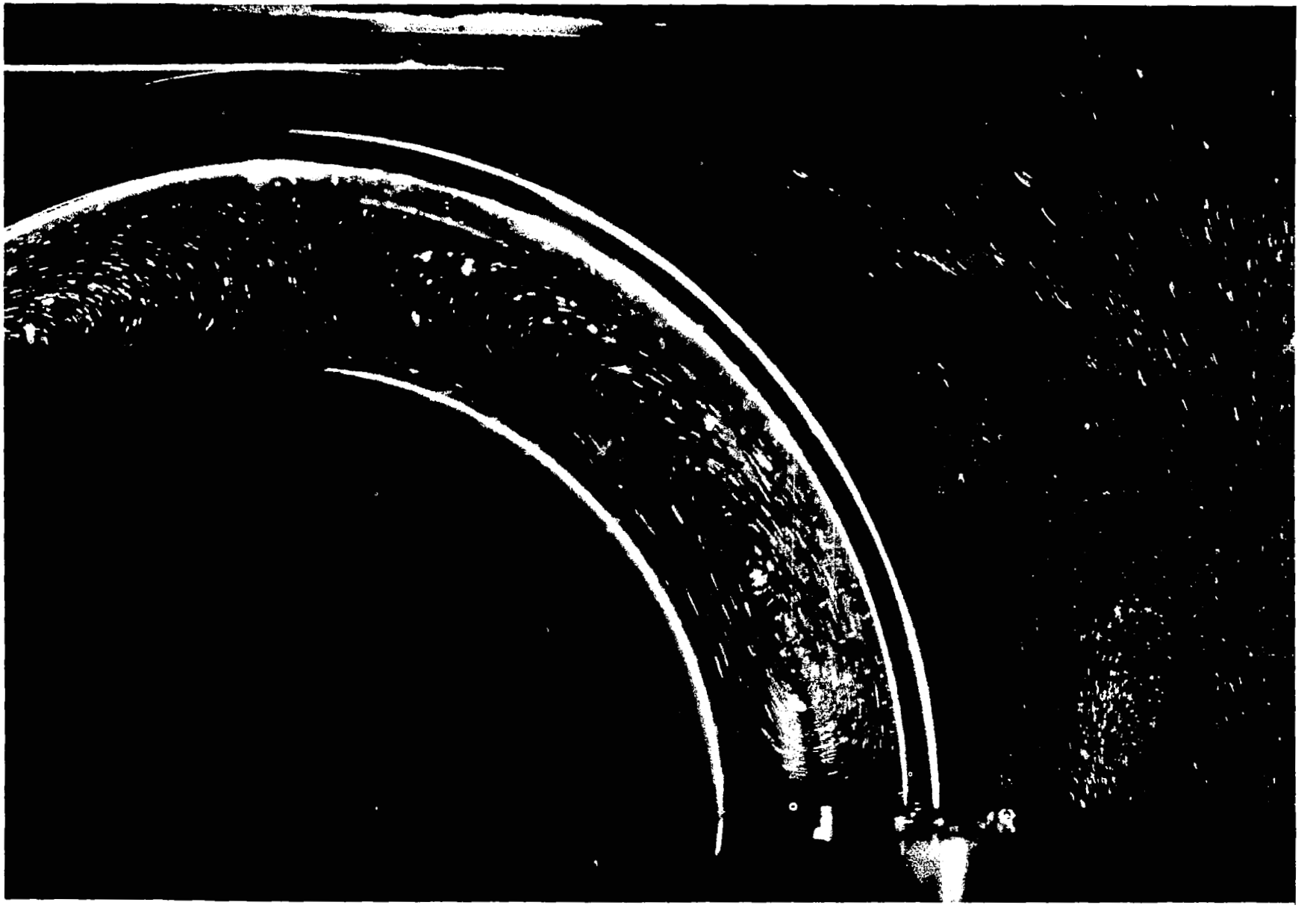

Figure 13. Experimental streak photograph. $\Delta V = 0$, $R_a = 11{,}000$.

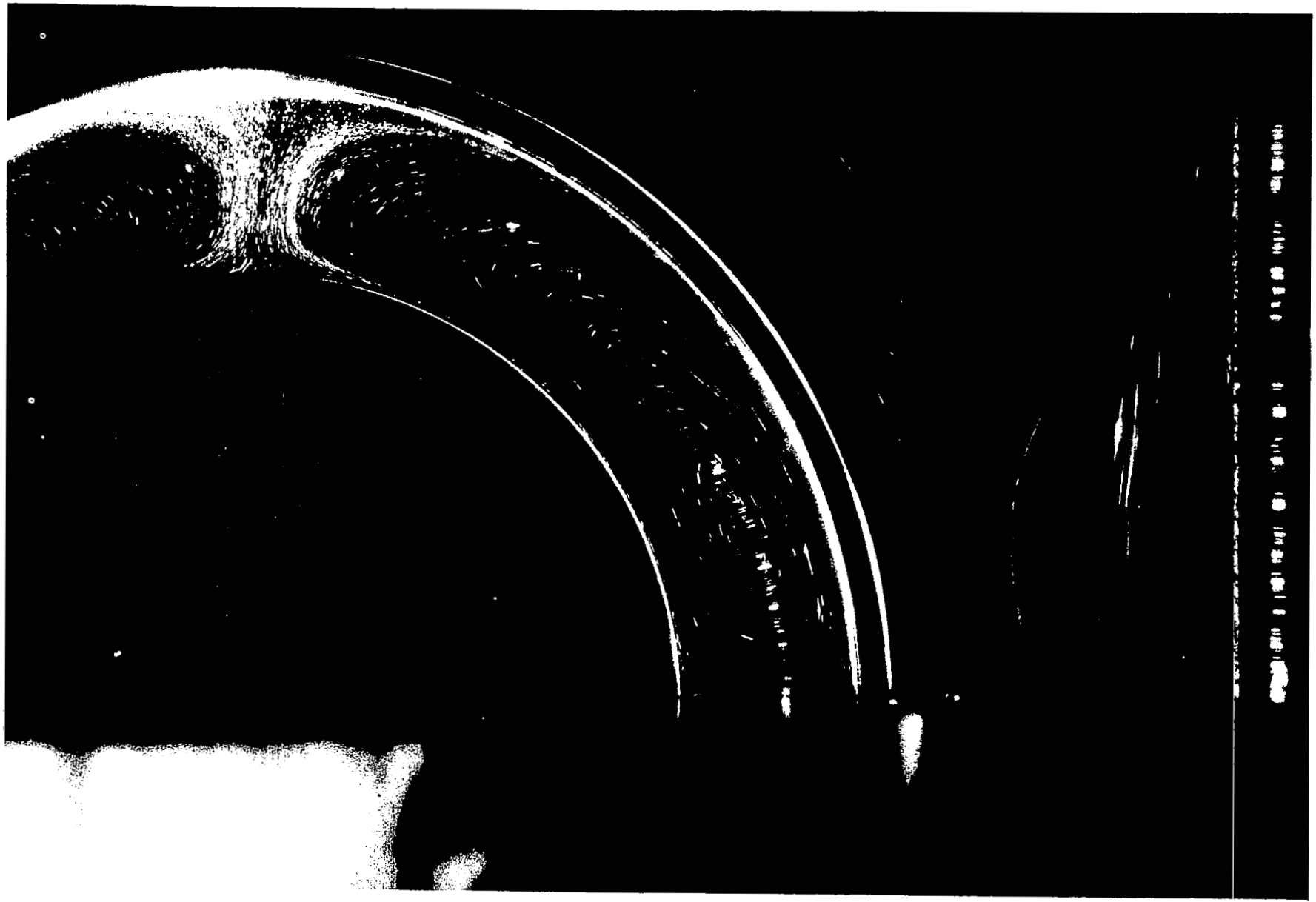

Figure 14. Streak photograph, $\Delta V = 0$, $R_a = 100{,}000$.

Figure 15. Comparison of theoretical and experimental (dots) latitudinal velocity $v(r,\phi)$ at $\phi = 20°$. $R_a = 45{,}000$.

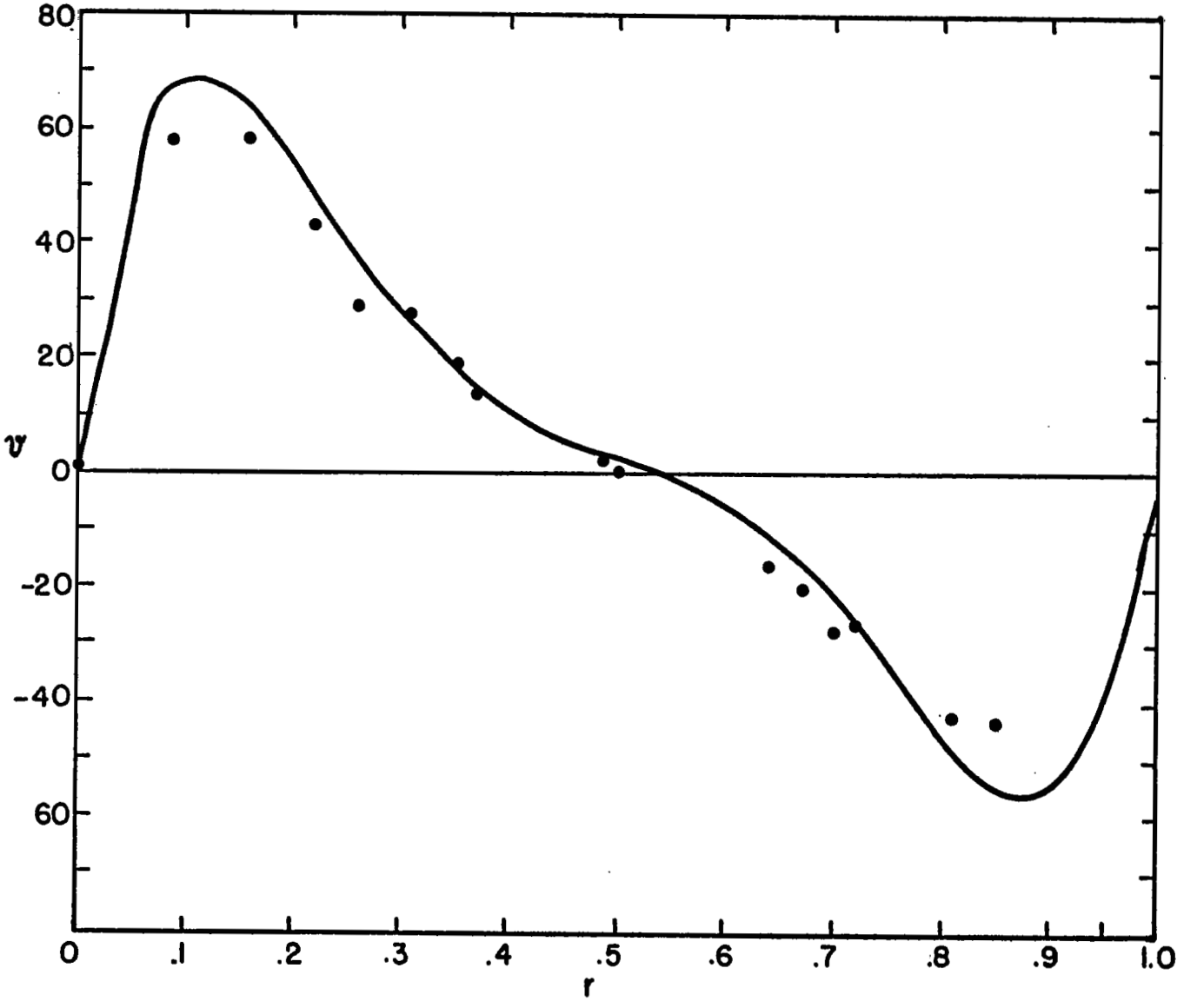

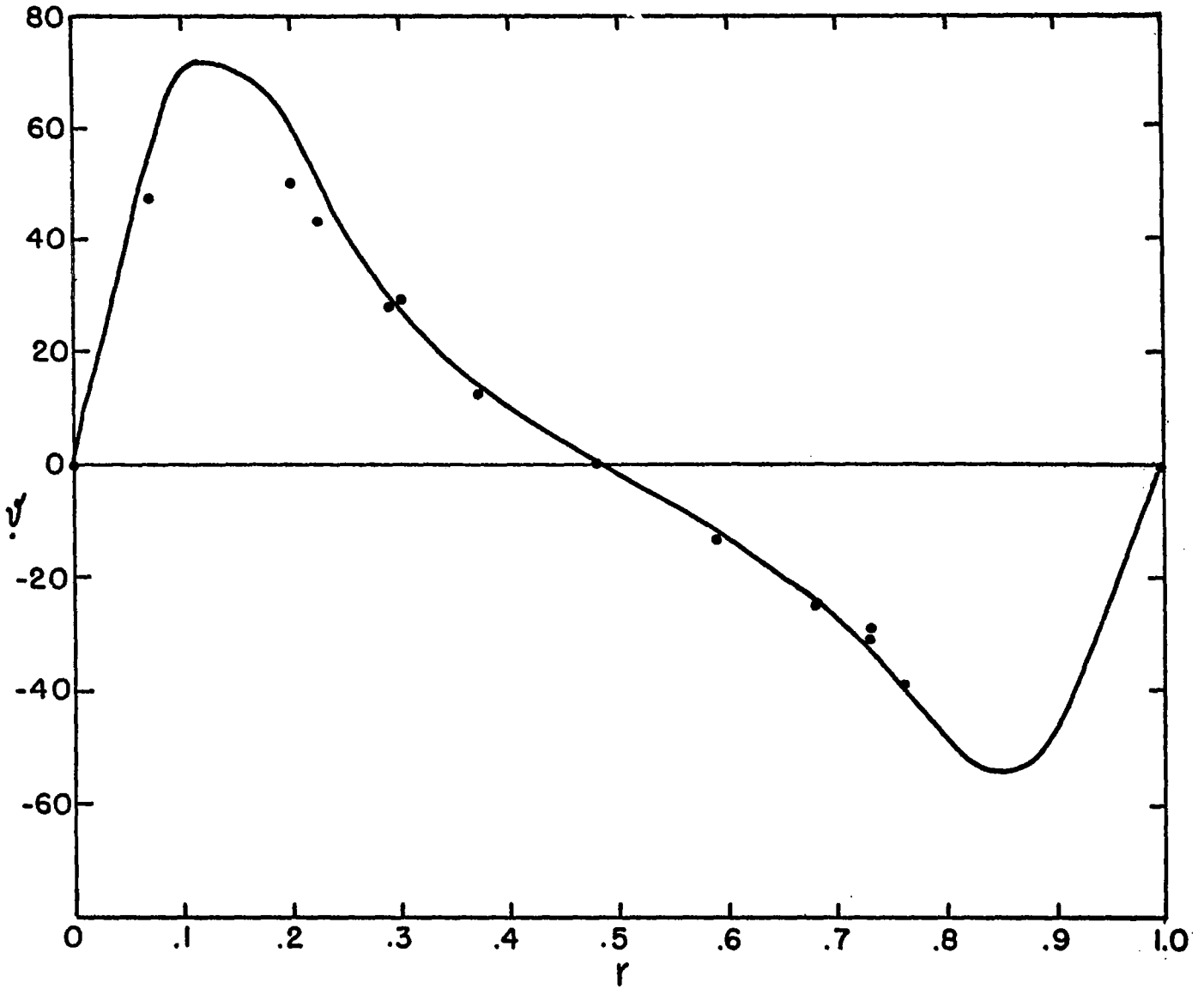

Figure 16. Comparison of theoretical and experimental (dots) values of v at $\phi = 30°$. $R_a = 45{,}000$.

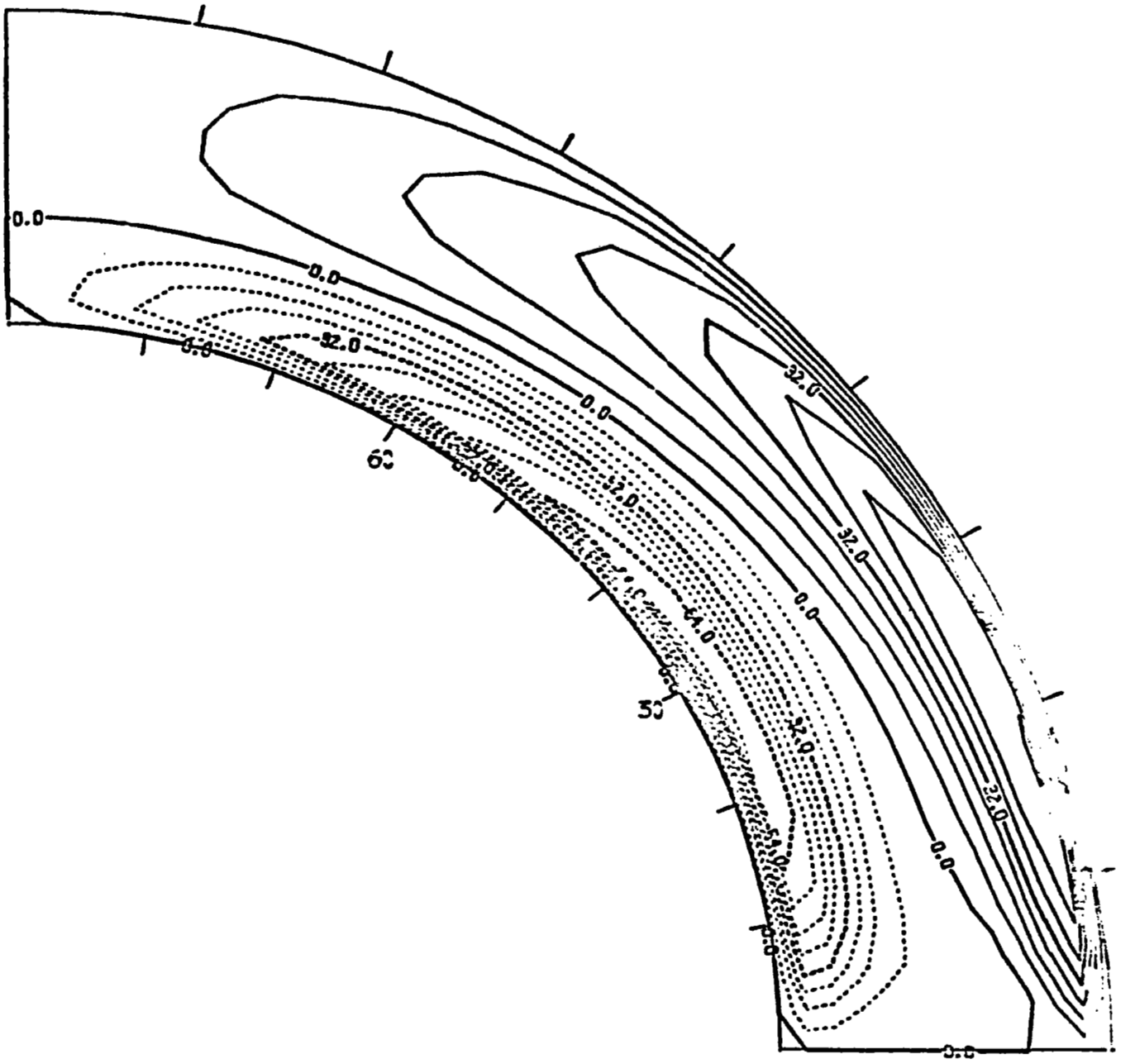

Fig. 17a. Contours of V (meridional velocity, dashed contours show negative values, i.e. directed towards the equator), for R_a = 45,000, ΔV = 0.

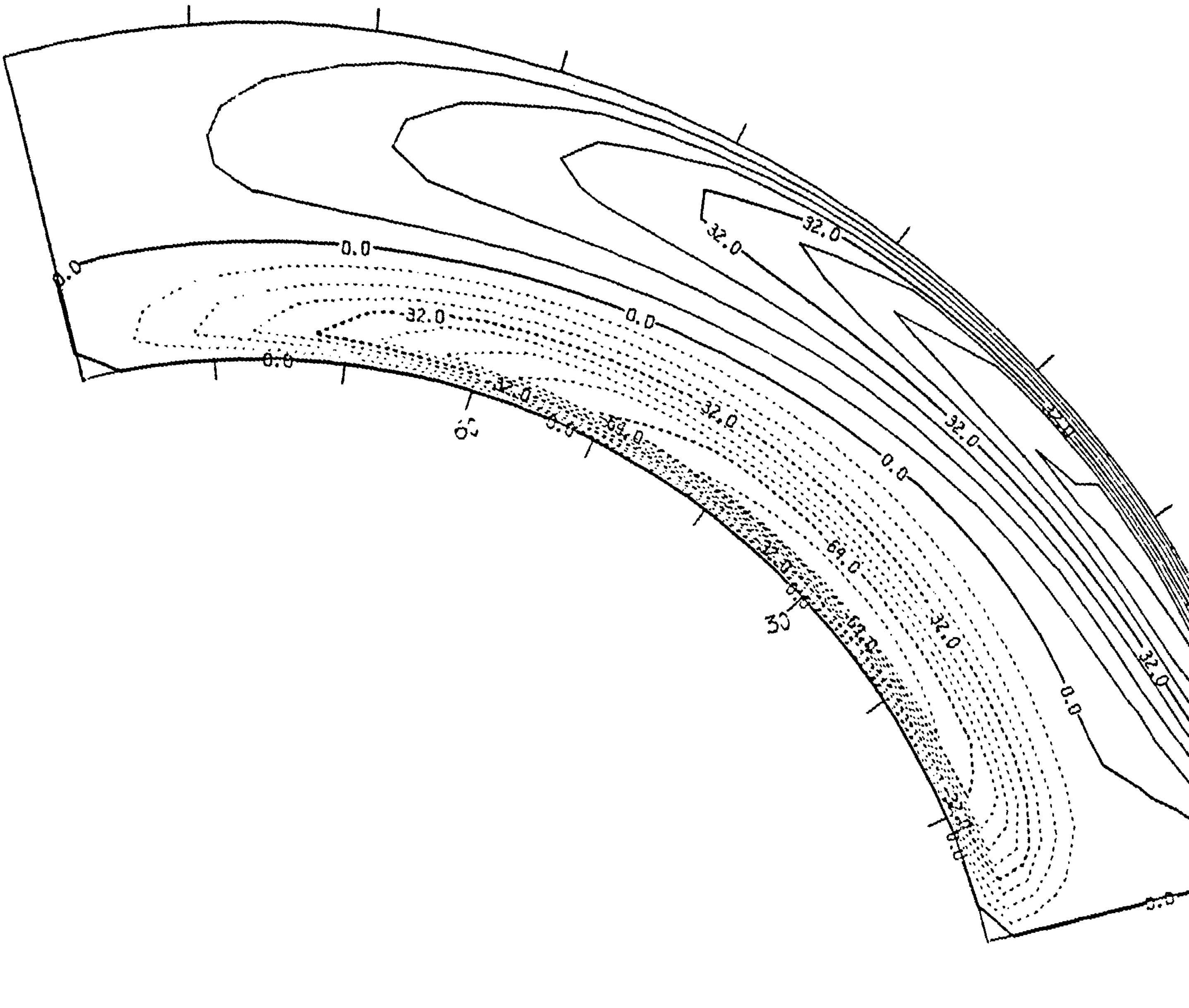

. . 15,000 volts.

nor would it arise in the zero gravity laboratory.

Figs. 18 show that the corresponding experimental circulations are nearly indistinguishable for $\Delta V = 0$ to 16 kv. Note how nicely the particles line up with the potential surfaces (e.g., compare figure 18b to figure 18a where the particles are winking at the camera). At fields of 8 kv or less particle tracking can be done. This is a major result. However, if one looks closely at fig. 18c, one sees evidence of 'dancing' particles near the inner sphere at the pole. The particles pick up space charge and move in the field. This motion sets a voltage upper limit to the use of this technique.

We have shown that flow measurements are possible at the fields needed in zero-g. We would also like a conclusive demonstration of the electrohydrodynamic effects in this geometry (to complement our previous demonstration and those of other workers mentioned in section 3). We have used the numerical model to suggest what we should look for. Fig. 19-20 show that at large field strength the circulation becomes multi-cellular. Near the pole cold fluid rises in response to the fact that the "gravity" has been reversed near the inner sphere (recall that $E^2 \simeq 1/r^4$ so electrodynamic forces are biggest at smaller r). There are also several 'plumes' (more obvious in fig. 20). These are thought to be electro-convective plumes, again with cold fluid rising, coming out of the boundary layer where "gravity" is inverted and being swept towards the equator by the main Hadley circulation. The time dependence can be seen by comparing figs. 21a and 21a. The 'plumes' are actually toroidal rolls moving equatorward.

It is suggested that future work be aimed at measuring the critical value of ΔV required for the first appearance of these electroconvective

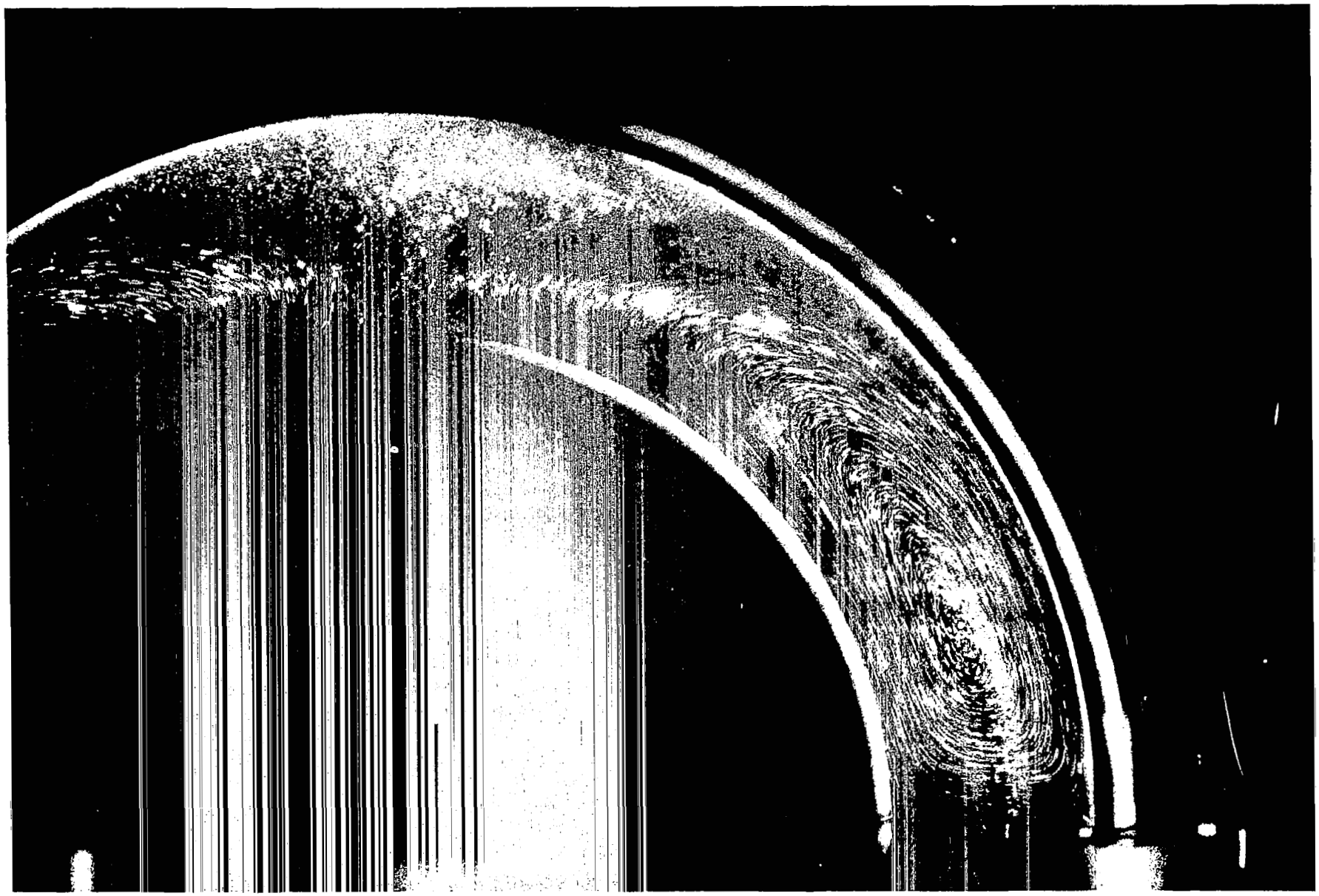

Fig. 18a. Experimental streak photographs for R_a = 45,000, ΔV = 0.

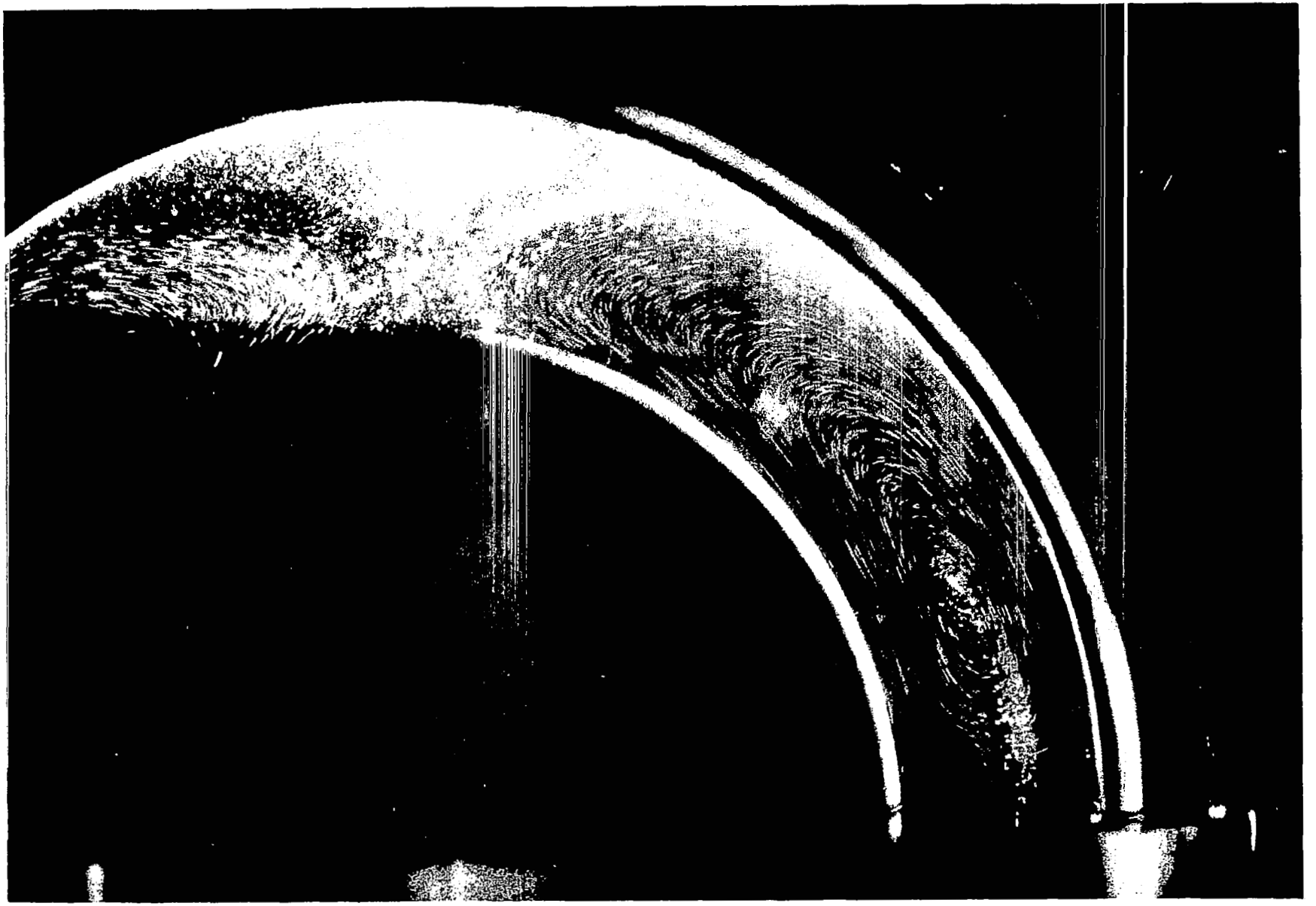

Fig. 18b. R_a = 45,000, ΔV = 8 kv.

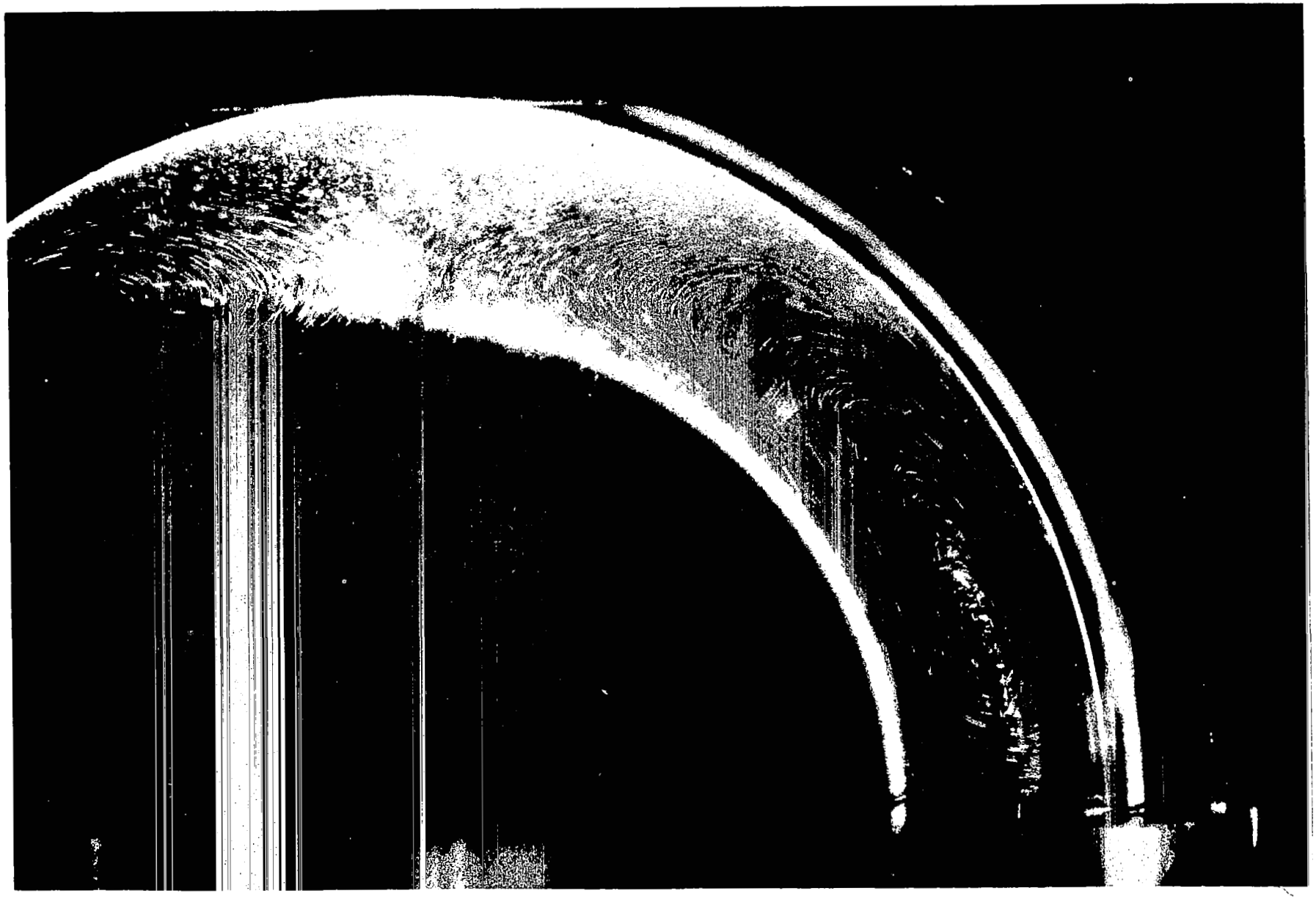

Fig. 18c. R_a = 45,000, ΔV = 16 kv.

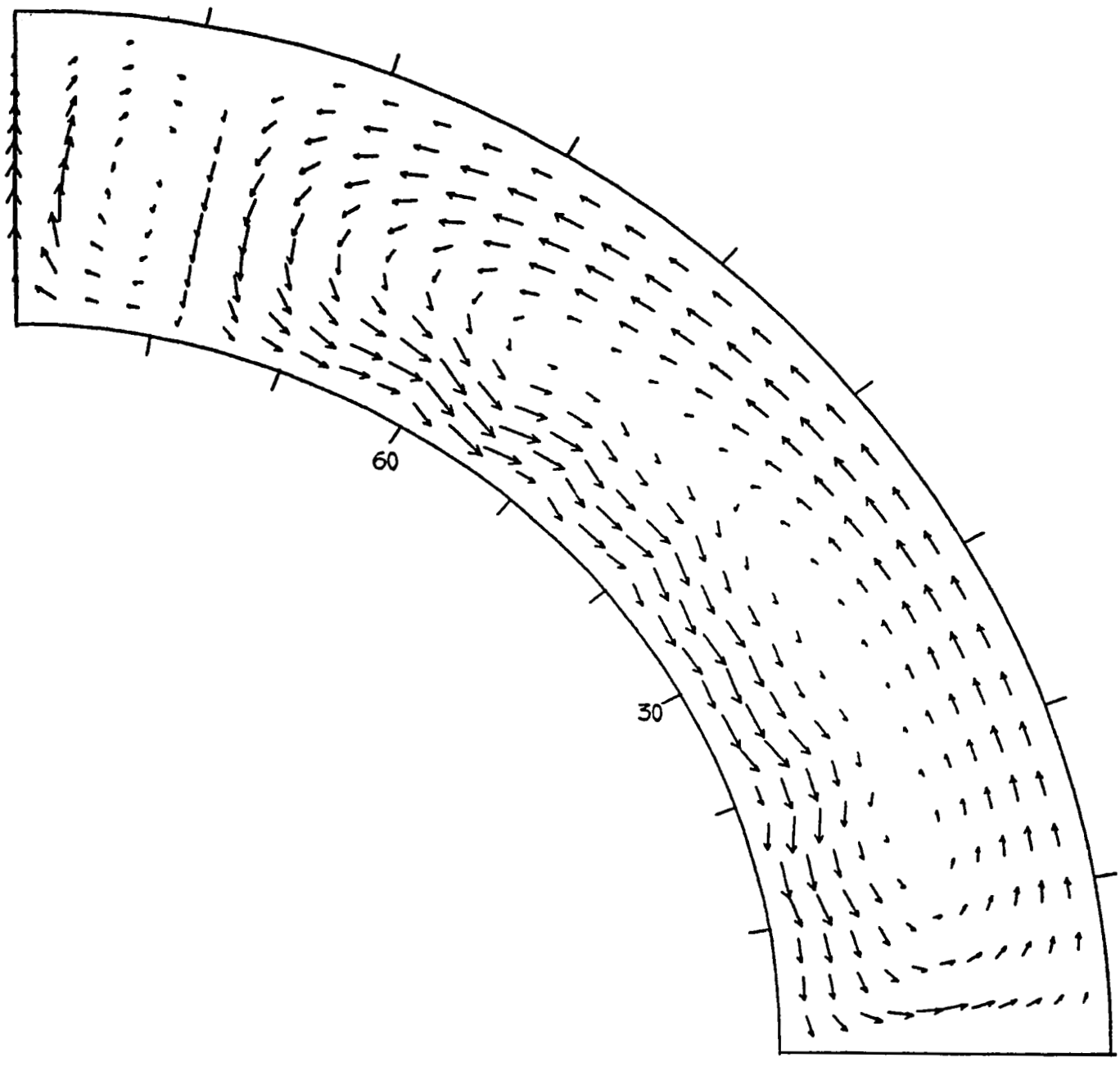

Fig. 19. Theoretical meridional circulation for R_a = 41,000. ΔV = 50,000 volts.

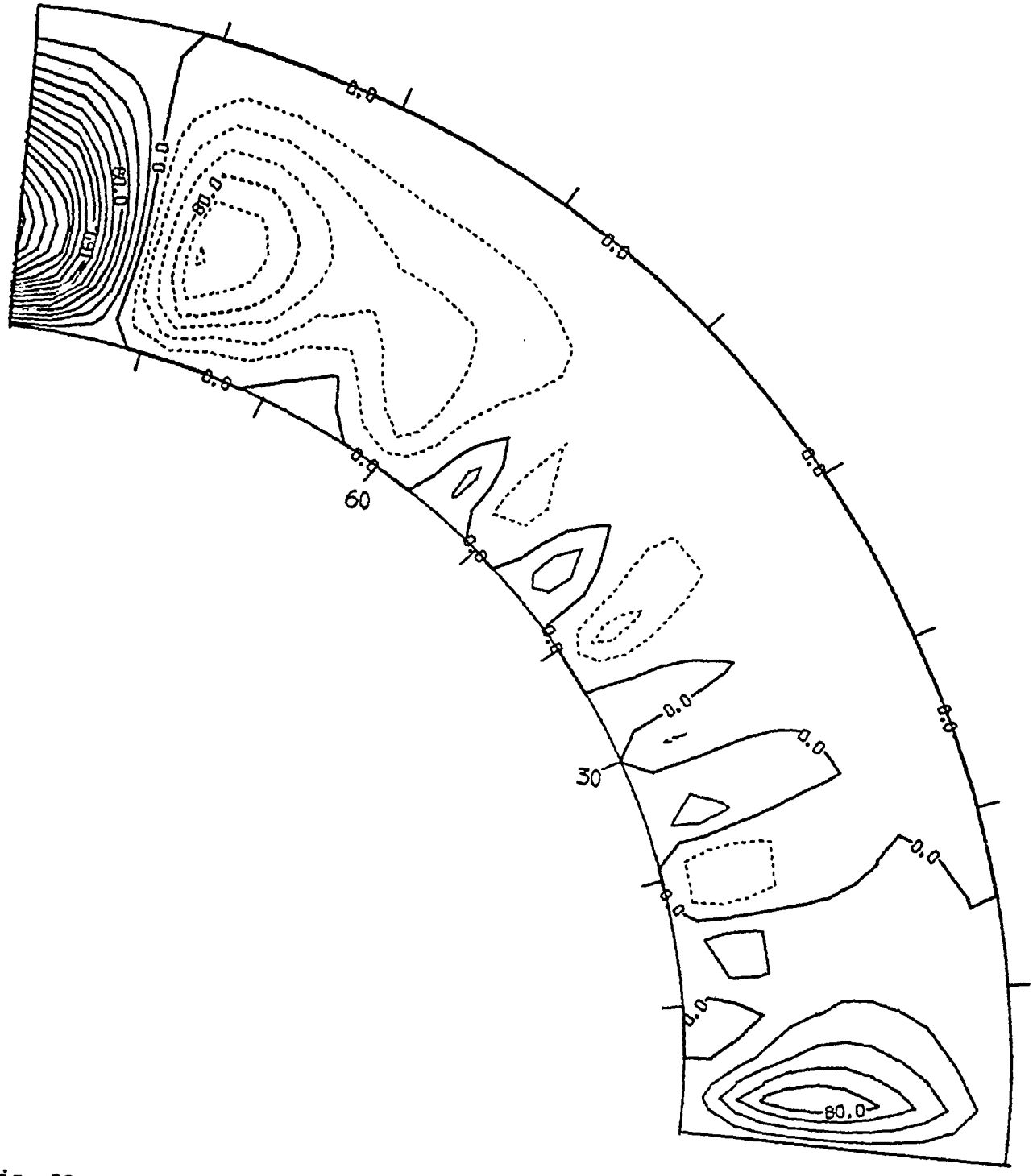

Fig. 20. Same as 19, except contours of dimensionless radial velocity.

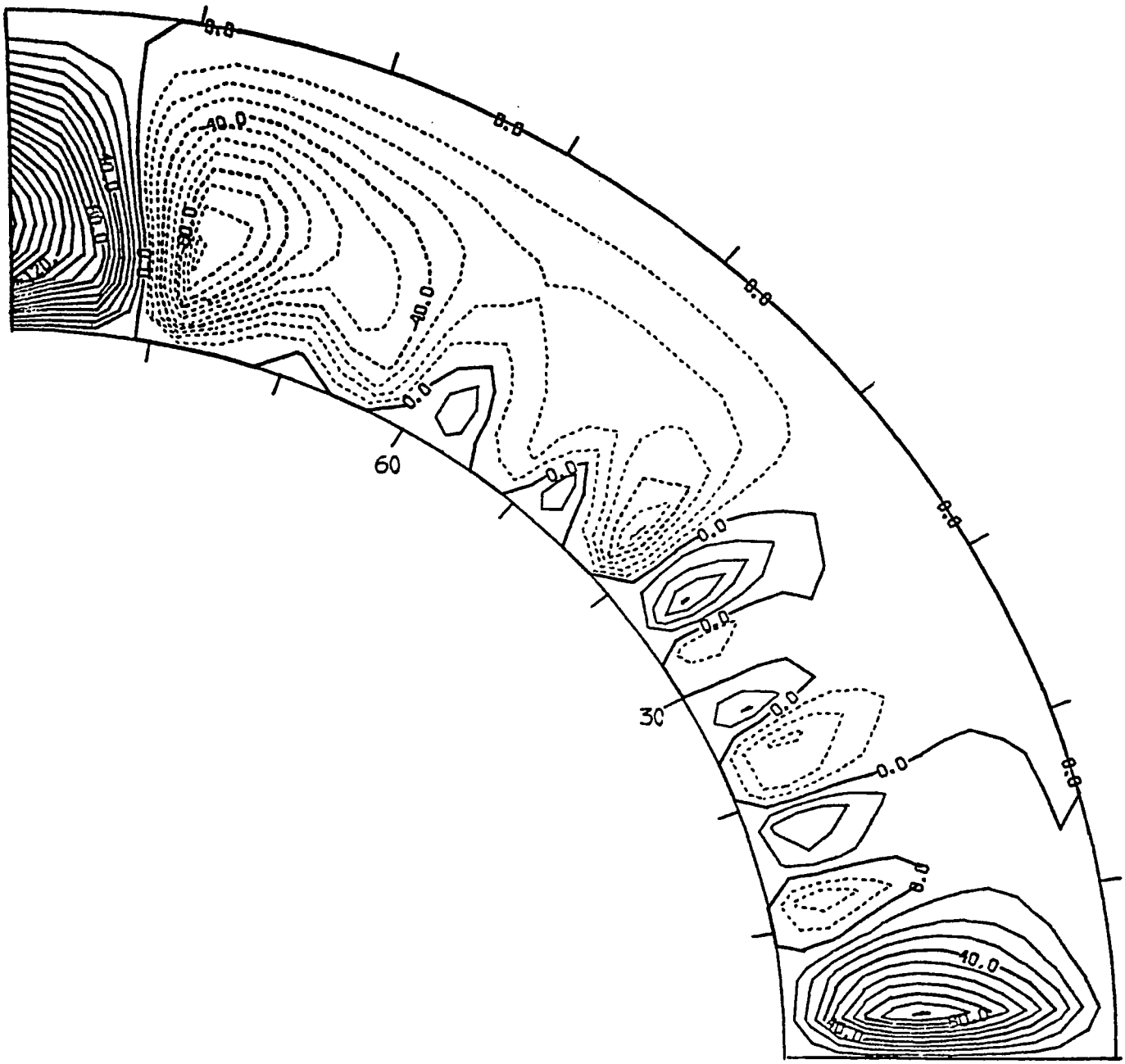

Fig. 21a. Radial velocity contour at time step 14,200. R_a = 41,000, ΔV = 50 kv.

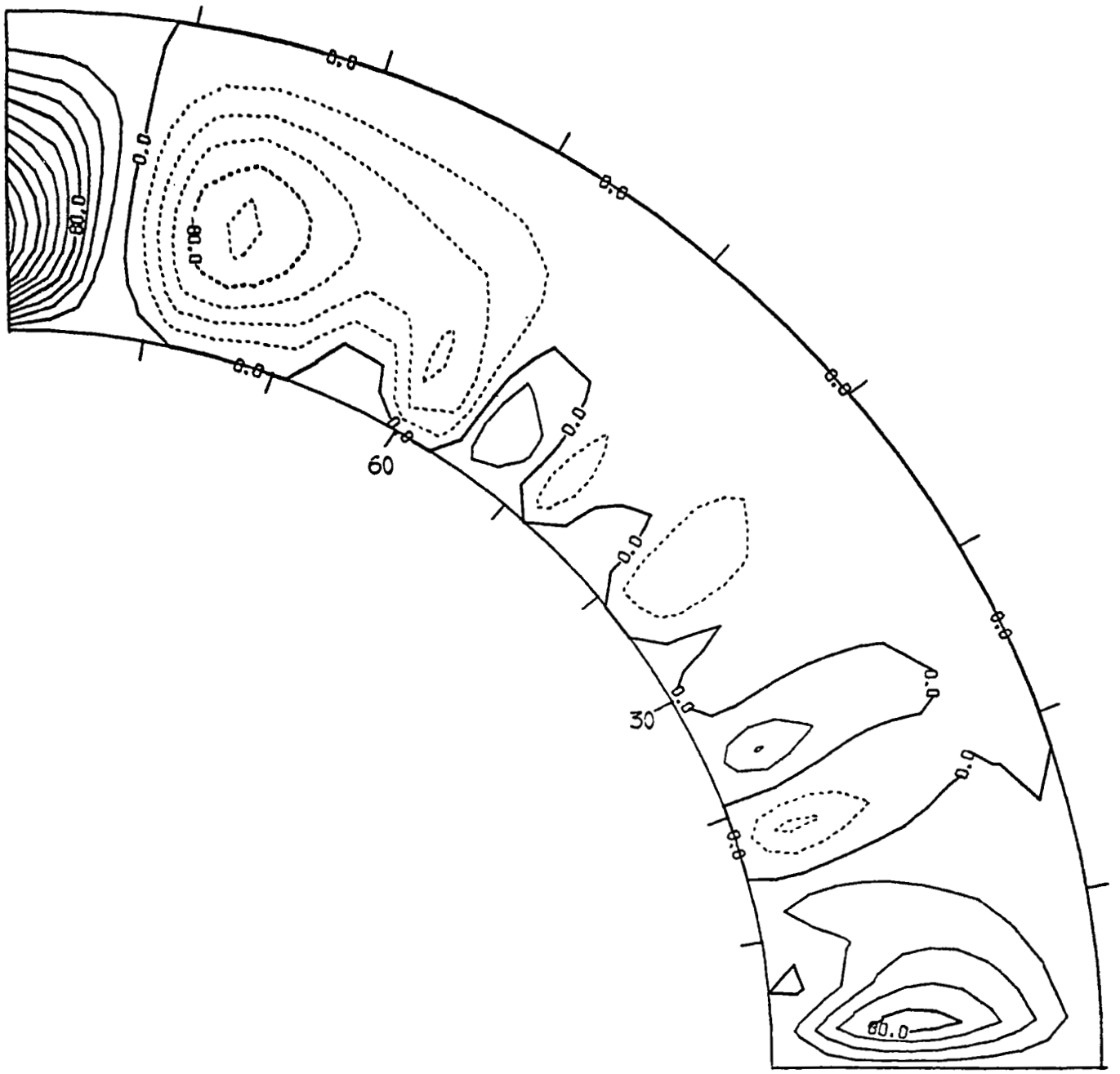

Fig. 21b. Same as 21a. Time step 15,000.

instabilities. For these axisymmetric modes the critical voltage is about 45 kv. This is beyond our capability at M.I.T. (We do have a 50 kv transformer at Colorado University where this work will be continued.) However, in the presence of the radial shear of the main Hadley cell the most unstable modes should not be axisymmetric toroids but poloidal banana rolls (e.g., $w' = w'(r,\theta)$, θ is longitude). Being more unstable they should occur at lower ΔV. During the continuation of this work at Colorado University we will compute the critical value of ΔV for poloidal rolls, and compare with experiment. Obviously the voltage will still be high; we anticipate something like 30 kv. Thus no particles can be used. We will measure the refraction of a laser beam reflected off the inner sphere as the apparatus turns slowly ($T_a << 1$). The rapid fluctuation of the reflected beam will indicate the presence of non-axisymmetric rolls. The critical value of ΔV and the observed wavelength will be compared with theory, thus obtaining an accurate measure of electroconvective effects in this geometry and checking out another possible visualization scheme.

7. Conclusions and recommendations for zero-gravity experimental design.

We have seen how terrestrial gravity effects swamp out electroconvective effects,and limit the application of this geophysical flow simulation method to low-g laboratories. Since the convective time scales are large an orbitting laboratory is preferred. It is easily seen that the apparatus cannot be too big because E-fields fall off as $1/r^2$. Thus the optimum size for the spherical annulus is a few centimeters for R_i and one or two cm for d. But as we saw in section 4, the Taylor number T_a can still be large enough so that experiments can be conducted in the rotationally dominated regions of parameter space.

Once the size (a few cm), temperature ($\lesssim$ 30°C) and voltage (< 8 kv) are set up, one might ask how big a feed-through neck is needed (see fig. 1). Alternatively one might ask how far away from the neck could one conduct experiments. The neck feeds high-voltage and coolent to the inner sphere so it must be on the order of a few millimeters in radius. Near the neck there will be fringing fields. If E^2 is not a function only of r there will be 'spurious' electroconvective buoyancy forces which are not radial, and hence that have no geophysical analogs. Thus we can only operate geophysical fluid dynamics experiments in that region of the spherical annulus where E^2 is almost radial, or where the electric potential ϕ is radial.

We have tried to estimate the neck influence region by solving Laplace's equation for the geometry of fig. 22. An inner sphere is at potential $\phi = 0$, and an outer sphere with a hole in it at angle Φ from the north pole, is at potential $\phi = V = 1$. Let θ be the angle measure from the pole downwards to the hole. Clearly we will be best off if $\theta = \Phi \to \pi/2$ or $d \to 0$. Figure 23 shows computed ϕ fields for several

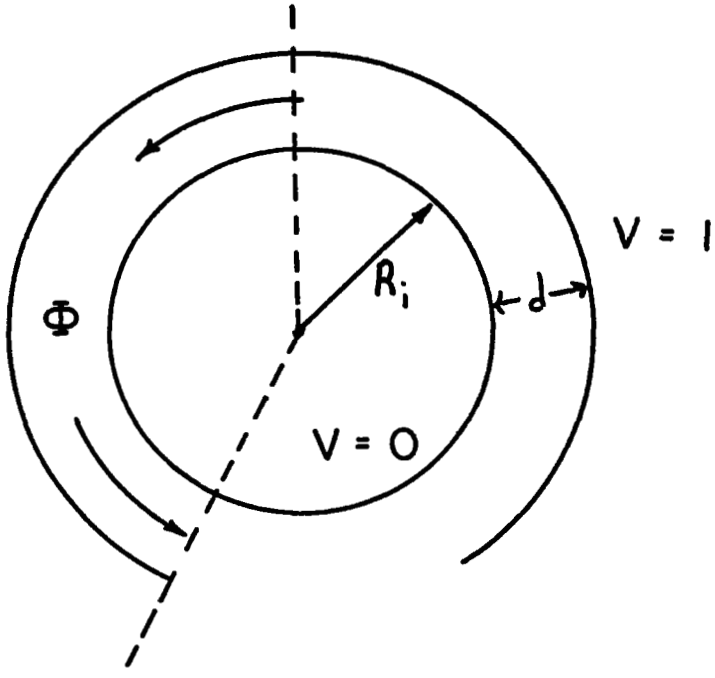

Fig. 22. Geometry for neck-effect calculations.

(a)

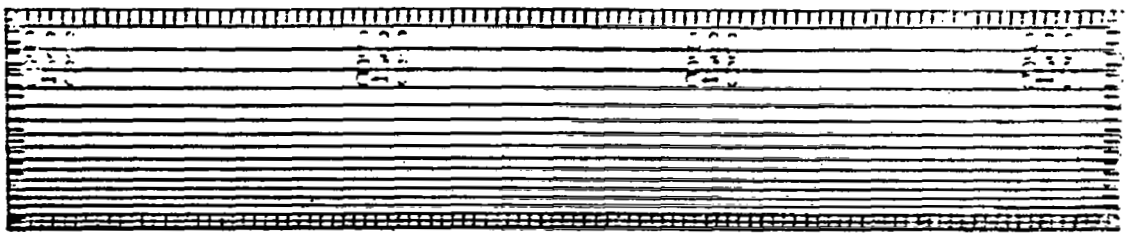

(b)

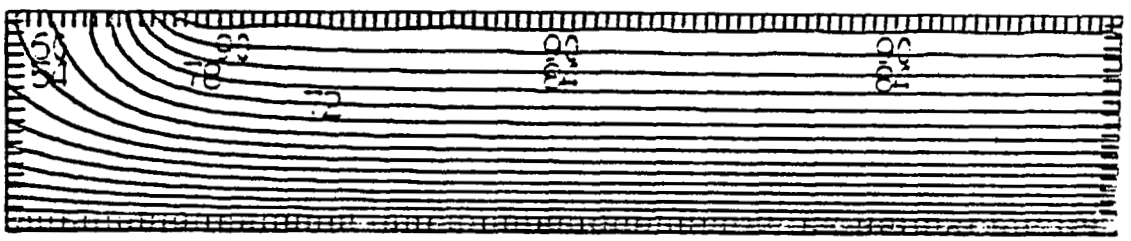

(c)

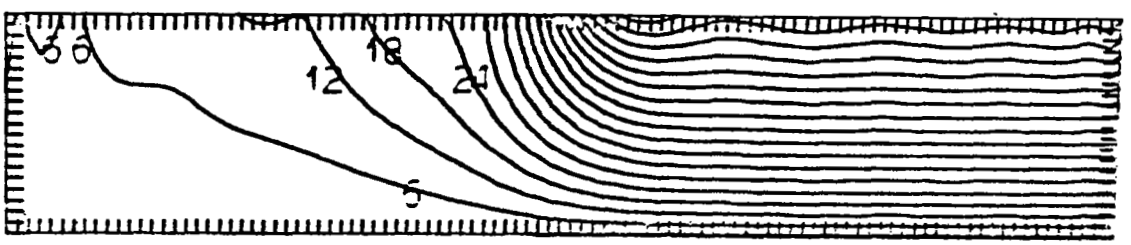

(d)

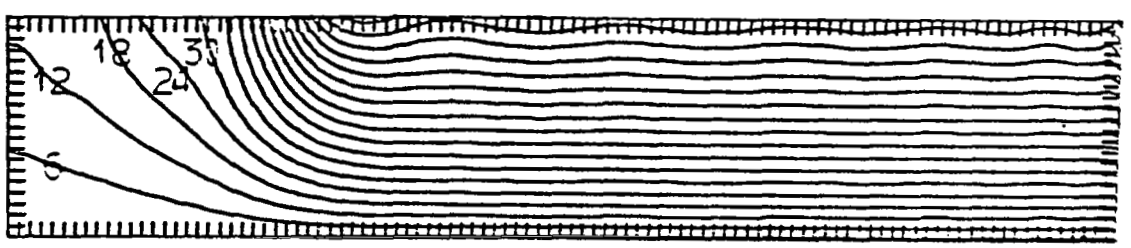

(e)

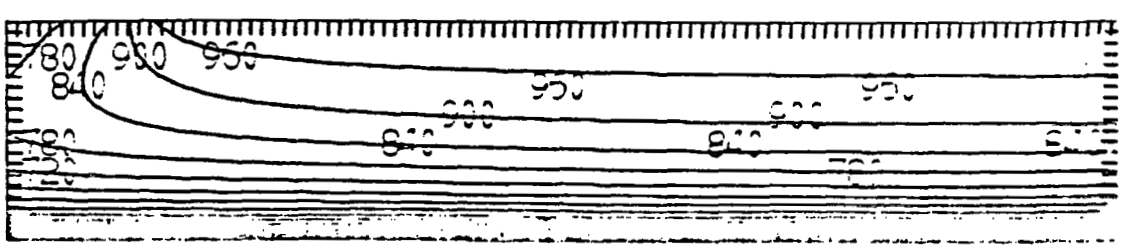

Fig. 23. Potential distributions. Horizontal axis is $x \equiv \cos\theta$. Neck is at $x = 1$, the left hand margin. Vertical axis is r. In a) $R_o/R_i = 1.25$, $\cos\Phi = -1$. In b) $R_o/R_i = 1.25$, $\cos\Phi = -.5$. In c) $R_o/R_i = 1.25$, $\cos\Phi = 0$. In d) $R_o/R_i = 2$, $\cos\Phi = -.75$. In e) $R_o/R_i = 8$, $\cos\Phi = -.75$. The right hand axis is at the north pole . Midway across each plot is the equator.

cases. It is obvious that if we confine ourselves to experiments in a hemisphere that there will be no problem (our typical experiment has $R_o/R_i \simeq 1.3$, $\cos\Phi \simeq -.83$). Looking at fig. 23b, equatorial annulus studies could conceivably be done to 45° S.

We have explored several visualization schemes for obtaining data on simulated flows in the spherical annulus geometry with electric fields applied. Some typical results are apparent from earlier photographs. They are:

a) particle tracks or streaks: useful for meridional flow structure and velocity. Can be used for low velocities (.1 mm/sec or less as observed here in fig. 14). Disadvantage: need to be injected if $g \neq 0$; otherwise will settle onto and adhere to surfaces. Only good for $\Delta V = 8$ kv or less.

b) Moiré (refractive index) photos: useful for planforms, wavelengths, frequencies and critical vlaues. Difficult for quantitative data. Good to breakdown point of the fluid. Best method for obtaining global structure of flow in longitude and latitude. Disadvantage: none. (Note other variants of this method may be better, e.g., shadow graph/Schlieren. Needs further technical study.)

c) Remote anemometry (Laser doppler): useful for direct measurement of flow velocity at single point. We have used this method with the spherical annulus and found the method to be reasonably easy to set up and align and gives accurate results if velocities $\gtrsim 1$ cm/sec are being measured. Otherwise vibration and alignment problems lead to noise problems. Considering the care required and the complexity of such systems, it is not recommended for space use, although it can be a useful tool for exploring the fluid dynamics of flows in the terrestrial laboratory relevant to this problem.

Figures 24 and 25 summarize current thought on a suitable zero-g experiment. It should be small and self-contained with the thermal 'bath' for the inner sphere and the high voltage power supply located in the rotating housing. The cell with some rough dimensions is shown in fig. 25. We very much prefer the visualization method of b) above. It is simple, reliable, inexpensive, and will serve to give in a direct photographic record all the necessary data on fluctuation plan-form (wave axis tilt, for example), wavelengths, wave slopes, etc. The outer surface will be cooled or heated with an air jet. Different cells are suggested for mountain barrier problems, problems with non-uniform heating on spherical surfaces; our sketch shows the simplest configuration which undoubtedly should be the first to fly in order to test out under actual zero-g conditions the concepts we have outlined and studied in this report.

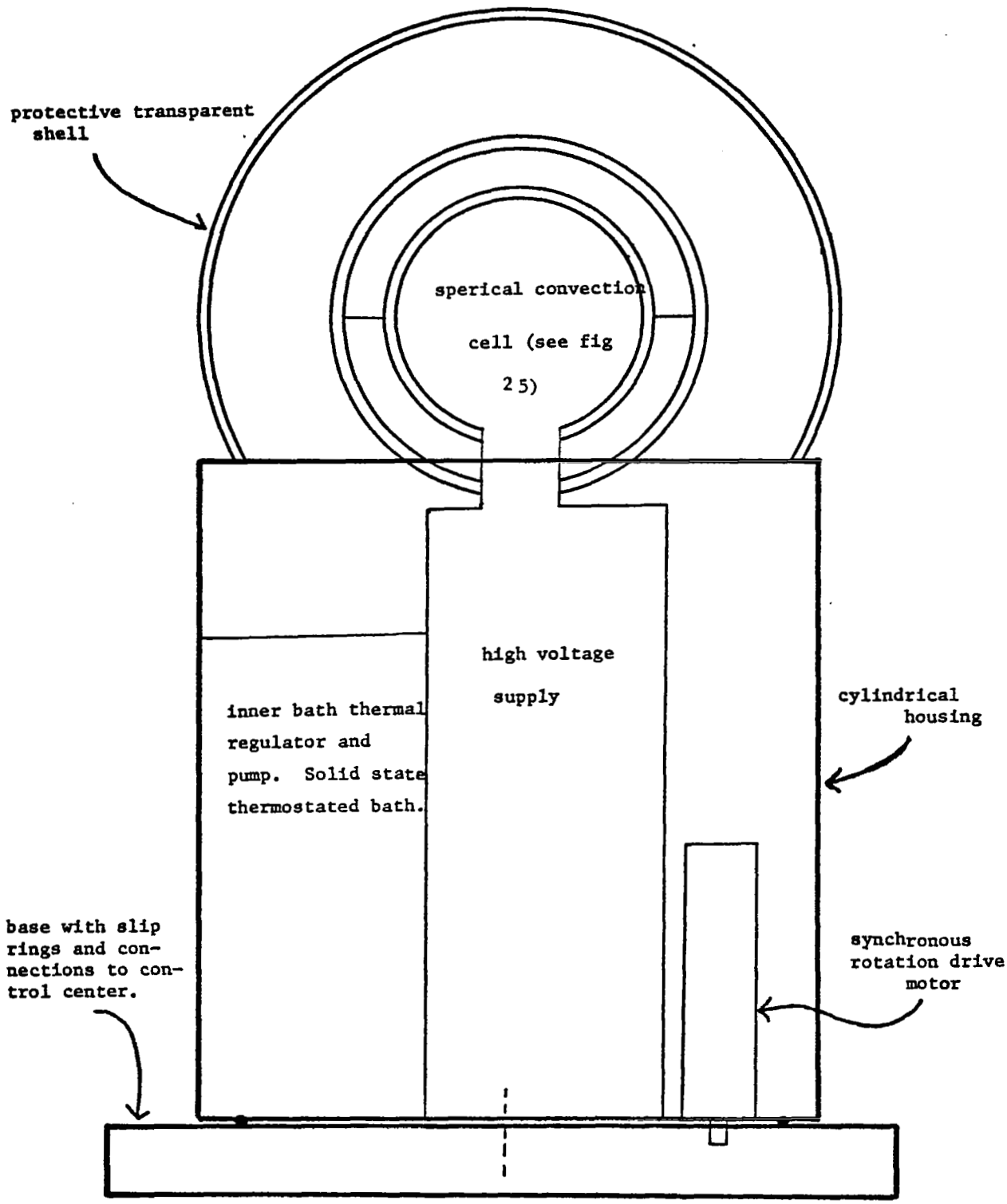

Figure 24. Sketch of electroconvection apparatus.

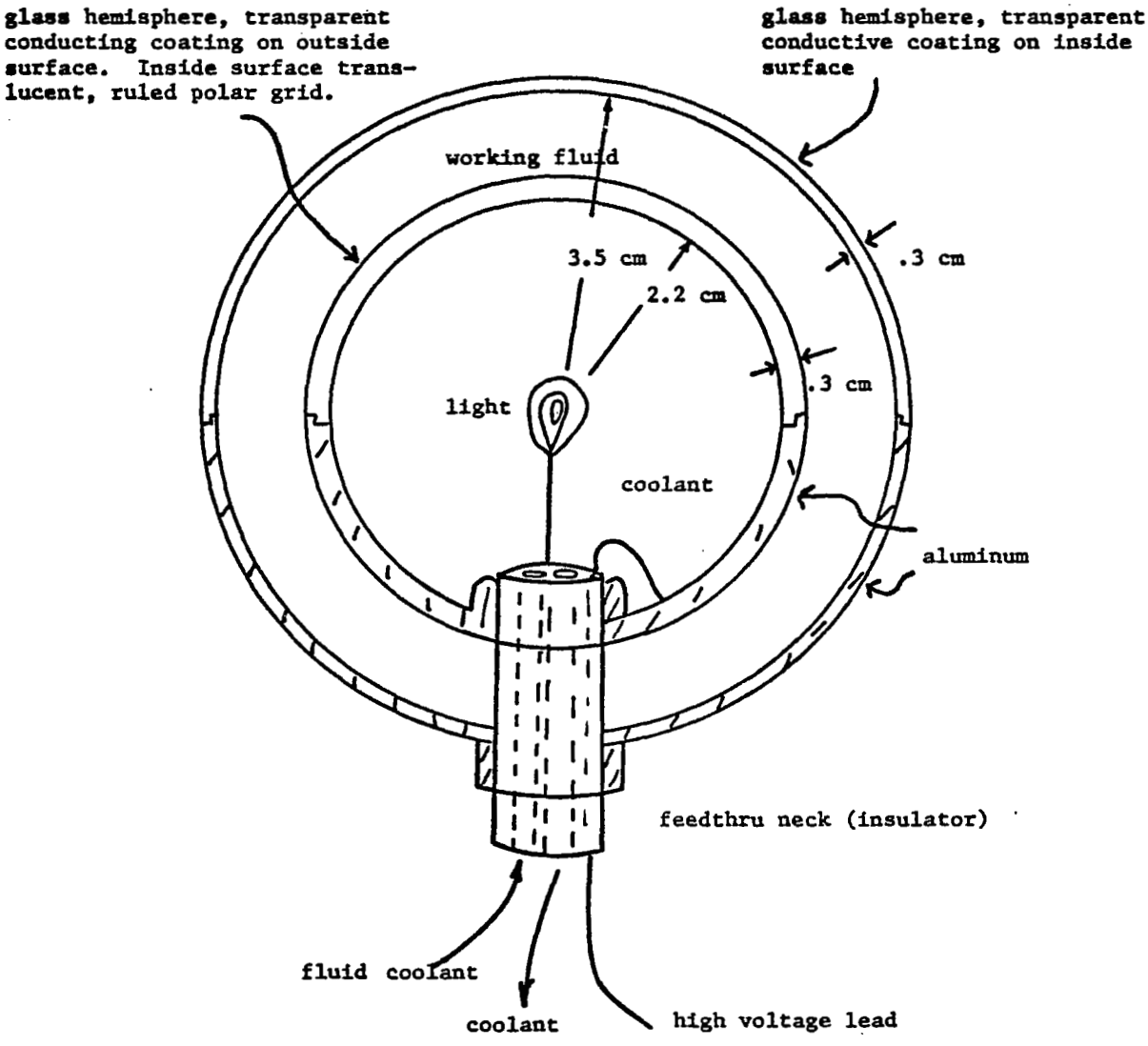

Figure 25. The electroconvection cell.

REFERENCES

Busse, F.H. 1970: Thermal instabilities in rapidly rotating systems. J. Fluid Mech., 44, 441.

Busse, F.H. & C.R. Carrigan 1974: Convection induced by centrifugal buoyancy. J. Fluid Mech., 62, 579.

Chandra, B. & D.E. Smylie 1972: A laboratory model of thermal convection under a central force field. Geophys. Fluid Dynamics, 3, 211.

Gilman, P.A. 1972: Nonlinear Boussinesq convective model for large scale solar circulations. Solar Physics, 27, 3.

Gilman, P.A. 1973: Convection in a rotating annulus uniformly heated from below. Part 2, Nonlinear results. J. Fluid Mech., 57, 381.

Gilman, P.A. 1974: Private communication.

Hart, J.E. 1972: A laboratory study of baroclinic instability. Geophys. Fluid Dynamics, 3, 181.

Melcher, J.R. & G.I. Taylor 1969: Electrohydrodynamics: a review of the role of interfacial shear stresses. Amer. Rev. Fluid Mech., 1, 111.

Turnbull, R.J. & J.R. Melcher 1969: Electrohydrodynamic Rayleigh-Taylor bulk instability. Phys. of Fluids, 12, 1160.

Turnbull, R.J. 1970: Thermal diffusion effects on electrohydrodynamic Rayleigh-Taylor instability, Phys. Fluids, 13, 2615.

Turnbull, R.J. 1971a: Instability of a thermal boundary layer in a constant electric field, J. Fluid Mech., 47, 231.

Turnbull, R.J. 1971b: Effect of a non-uniform alternating electric field on the thermal boundary layer near a heated vertical plate, J. Fluid Mech., 49, 693.

Williams G.R. & J.B. Robinson 1973: Dynamics of a convectively unstable atmosphere: Jupiter?. J. Atmos. Sci., 30, 684.

NASA-Langley, 1976